Flux phase as a dynamic Jahn-Teller phase: Berryonic matter in the cuprates

R. S. Markiewicz and C. Kusko
Physics Department and Barnett Institute, Northeastern University, Boston, Massachusetts 02115
(Received 15 October 2000; revised manuscript received 14 February 2002; published 1 July 2002)

There is considerable evidence for some form of charge ordering on the hole-doped stripes in the cuprates, mainly associated with the low-temperature tetragonal phase, but with some evidence for either charge-density waves or a flux phase, which is a form of dynamic charge-density wave. These three states form a pseudospin triplet, demonstrating a close connection with the $E\otimes e$ dynamic Jahn-Teller (DJT) effect, suggesting that the cuprates constitute a form of Berryonic matter. This in turn suggests a new way of looking at the DJT effect: we provide an interpretation in terms of *abstract operator algebra*, demonstrating (1) a purely electronic DJT effect and (2) a generalization of the DJT effect applying to a wide category of competing instabilities. A simple model of the Cu-O bond stretching phonons allows an estimate of electron-phonon coupling for these modes, explaining why the half breathing mode softens so much more than the full oxygen breathing mode. The anomalous properties of O^{2-} provide a coupling (correlated hopping) which acts to stabilize density wave phases.

DOI: 10.1103/PhysRevB.66.024506 PACS number(s): 74.20.Mn, 71.38.−k, 63.20.Kr, 71.45.Lr

I. INTRODUCTION

Recently, there has been considerable interest in the possibility of an anomalous phase arising in the cuprates—variously called the flux,[1–3] orbital antiferromagnetic,[4,5] or *d*-density wave[6] phase—and having a finite orbital angular momentum in its ground state. Here, we demonstrate that flux phases can be generated via a solid-state analog of the dynamic Jahn-Teller (JT) effect, closely related to the concept of ''Berryonic matter.''[7]

In a (molecular) JT effect, an electronic degeneracy in a symmetric molecule is lifted by distorting the molecule and lowering the free energy by an amount E_{JT}. A *dynamic* JT (DJT) effect arises when there is a degeneracy both of electronic levels and of molecular vibrations (strictly speaking, when two independent distortions have the same JT energy lowering). Quantum tunneling between the two distortions restores the (time-averaged) symmetry of the molecule, but leads to a net orbital angular momentum which is half-integrally quantized.[8,9] In principle, an analog of the DJT effect should exist in dense solids,[10,11] but this feature of ground state nuclear motion has not been adequately described. Here the connection between DJT effects and flux phases is worked out. In particular, the anomalous π phase is just the Berry phase of the DJT effect.

This result is particularly timely, since DJT effects have been proposed to play a role in a number of materials of current interest, including buckyballs,[12,7] cuprates,[13–15] and manganites.[16] Remarkably, many of these materials display stripe phases and/or high-temperature superconductivity, and it has been proposed that either strong electron-phonon coupling[17,18] or flux phases may be responsible for these features. Moreover, in the cuprates, there is recent evidence for both strong phonon anomalies[18–24] and possibly the flux phase.[25] Hence, the present formalism is applied to a simple model of the in-plane phonons in the cuprates.

The two JT modes plus the DJT state can be combined into a ''pseudospin'' triplet[26] of charge-density wave (CDW), bond order wave (BOW), and flux phase (dynamical CDW). Restricted to a single four-copper-plaquette ''molecule,'' they reduce to an $E\otimes(b_1+b_2)$ JT problem. The CDW and BOW can be related to important phonon modes in the cuprates: namely, the oxygen breathing mode and a shear mode which couples to the tilting mode associated with the low-temperature tetragonal (LTT) phase. (The electronic modes are illustrated in Fig. 1, below, and the corresponding phonons in Fig. 2.) A formal definition is given of the DJT effect in terms of an abstract operator algebra. This definition generalizes to provide an analog to the DJT effect for a variety of competing instabilities in solids.

Our model calculations find a crossover from an antiferromagnetic insulator at half filling to a doped paramagnetic phase stabilized by density wave order, separated by a regime of phase separation (probably related to stripes, as discussed in Appendix A). The density wave is predominantly stabilized by an electron-electron interaction, but with a significant structural component. Hence, the phonons can be considered as weakly coupled spectators, which can be used to probe the predominantly electronic interactions. The system is close to but probably not at the DJT degeneracy point, with the shear and flux phases lying lowest in energy.

This paper is organized as follows. Section II surveys the various phonons which experimentally are found to couple to the holes and shows that they fall into two classes, which couple strongly to electronic CDW's and BOW's, respectively. In particular, the BOW couples strongly to LTT and dimpling distortions. (In Appendix A additional evidence is presented that the coupling is particularly strong in the hole-doped regions, e.g., on charged stripes.) Section III A shows that these CDW's have a well-defined group (pseudospin)

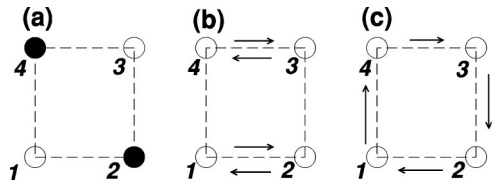

FIG. 1. Pseudospin triplet: O_{CDW} (a), O_{BOW} (b), and O_{OAF} (c).

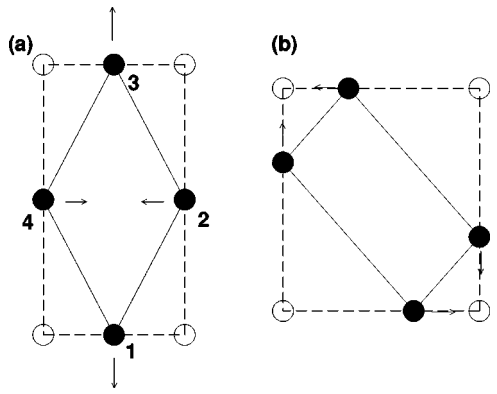

FIG. 2. B_1 (a) and B_2 (b) distortions of Cu_4O_4. Open (solid) circles represent the Cu atoms (O atoms).

structure, which can lead to a flux phase via competition between these modes. This is closely related to the DJT effect of a square molecule (Sec. III B). Section III C generalizes the pseudospin formalism to a lattice. Section III D provides a different generalization. By restating the DJT effect as a general property of quantum operator algebras, it is seen that related effects can arise in many situations of *competing order parameters*, including the SO(5) model. As a result, a number of alternative routes to flux phases are described.

In Sec. IV the DJT model is applied to the cuprates, both for purely electronic interactions (Sec. IV A) and for combined electron-electron and electron-phonon coupling (Sec. IV B), and it is found that the anomalous behavior of the O^{2-} molecule leads to a particular form of *correlated hopping* which helps stabilize paramagnetic CDW phases. Appendix B discusses electron-phonon coupling to a large number of planar bond stretching modes, using both three band (Appendix B 1) and one band (Appendix B 2) models. The reason why the half breathing mode is so strongly renormalized is explained. Some discussion of *desiderata* for a more complete model are presented in Sec. V, and conclusions are presented in Sec. VI.

II. CLASSIFICATION OF PHONON MODES

A. Two groups of phonons

There is considerable evidence for strong electron-phonon coupling effects in the cuprates. While the effects are weaker than in the nickelates and manganites, we postulate that it is this relative weakness which allows superconductivity to compete against charge ordering. The difficulty in analyzing the coupling lies in the fact that it is spread over so many different modes, and the modes vary from cuprate to cuprate. Here we show that the strongly coupling modes can be classified into two groups, depending on the electronic states they couple to. These electronic states can be described as site CDW's (leading to a pileup of charge on alternate Cu atoms) vs bond CDW's (pileup on oxygens)—for short, CDW's vs BOW's—illustrated in Fig. 1. Alternatively, since the modes both couple strongly to a Van Hove singularity (VHS), they may be classified by how they split the VHS peak: the site CDW's leave the X and Y $[(\pi,0)$ and $(0,\pi)]$ point VHS's equivalent, but split each (as in the one-dimensional Peierls transition); the bond CDW's make the X and Y points inequivalent.

It is the dynamic coupling of both of these modes which can give rise to flux or orbital antiferromagnetic (OAF) phase, Fig. 1(c). CDW's can be instrumental in driving phase separation instabilities in the cuprates, and evidence specifically linking these phonons to the charged stripes is presented in Appendix A.

The phonons coupling strongly to the site CDW's are the well-known oxygen breathing modes, which play an important role in several models of the cuprates.[27,14,17,28,29] These modes are found experimentally to couple strongly to the doped carriers in both $La_{2-x}Sr_xCuO_4$ (LSCO) and $YBa_2Cu_3O_{7-\delta}$ (YBCO).[30] However, while theoretically the strongest coupling should be at (π,π), experimentally breathing modes appear more strongly coupled near $(\pi,0)$. There is considerable evidence for coupling to stripes, presented in Appendix A.

B. Relation of shear mode to LTT, Dimpling, etc.

Less attention has been paid to a second class of phonon modes, which split the degeneracy of the X and Y VHS's. Whereas theoretically there should be a strong electron-phonon coupling with *bond stretching* modes, the observed soft modes are *bond bending* modes, with different modes in each family of cuprates: the low-temperature orthorhombic (LTO) and LTT tilts in LSCO, a dimpling mode in YBCO, and a rotation of the four planar oxygens about the central Cu in the electron-doped cuprates.[31] Here, we suggest that there is a connection between these modes and the shear instability. We discuss each family of cuprates separately.

LSCO. Direct evidence for proximity to a shear mode instability has been noted in LSCO near the 1/8th anomaly, in the form of softening of the C_{11}-C_{12} elastic modulus.[32] The strongest indirect coupling to the shear is via the tilt mode associated with the LTT distortion, perhaps the most important mode in the cuprates after the breathing modes. This mode (1) couples strongly to the VHS and (2) plays an important role in stripe physics. It has been suggested that the observed LTO phase in doped LSCO is really dynamically disordered, with the local order being closer to LTT.[15] Evidence for this (and its connection to stripe phases) is presented in Appendix A.

While this tilt mode is the soft mode of the LTT distortion, it is important to keep in mind certain distinctions between the two. Thus, an important driving force in both LTO and LTT instabilities is lattice mismatch between the CuO_2 and LaO layers. In the instability, this mismatch is partially relieved by *reducing the Cu-Cu separation*; the tilt moves the intervening oxygen aside, allowing a closer Cu-Cu approach. On the other hand, the pure optical phonon mode is defined as a relative motion of the atoms within a unit cell. Hence the tilt mode *involves only oxygen motion, the Cu-Cu separation remaining unchanged*. With this distinction in mind, we briefly demonstrate that the phonon mode does split the VHS degeneracy and, hence, couples to the BOW. Since the Cu-Cu separation a remains unchanged, the Cu-O separation

must increase to $d=a/(2\cos\theta)$, where θ is the angle by which the oxygen is tilted out of the plane of the coppers. Lifting the oxygen also decreases overlap between the Cu $d_{x^2-y^2}$ orbital and the oxygen p_x orbital, by a factor $\cos\theta$. Since the Cu-O hopping parameter is approximately $t_0 \sim \cos\theta/d^{3.5}$, the effective Cu-Cu hopping is $t \sim t_0^2 \sim \cos^9\theta$. For the LTT mode, the tilts are only in one direction, leading to $t_x \neq t_y$, thereby coupling to the BOW. A similar effect arises for the full LTT distortion.[33] Qualitatively, the LTT tilt pattern arises because the CuO_6 octahedra tilt as rigid units:[34] since the octahedra are corner sharing, alternate octahedra must tilt in opposite directions, leading to a distortion at wave vector $\vec{Q}=(\pi,\pi)$. (The detailed interpretation involves partial hole localization on oxygens, and the large size difference between O^- and O^{2-}.[33]) Such VHS splitting has recently received renewed interest.[35,36]

YBCO. While there was an early report of a local tilt-mode instability in YBCO,[37] it is more likely that the role of the LTT distortion is taken by the *dimpling mode*. While this mode involves predominantly copper and oxygen motion out of the CuO_2 planes, it also couples to in-plane Cu-O displacements. In particular, it couples to the orthorhombicity[38] and, hence, to the same shear mode involved in the LTT phase (distortion B_1 in Fig. 2 below). Hence the dimpling also splits the VHS's, but in a different pattern.[39] Experimentally, the distortion competes with superconductivity, and a large decrease of the orthorhombicity is found both at and below T_c,[40] while a discontinuous change in the dimpling is found on passing through optimal doping.[41] *Chain ordering* also plays a role, since it splits the degeneracy of the VHS's along and across the chain direction. Photoemission seems to find that the VHS along $X(Y)$ is below (above) the Fermi level,[42] while neutron scattering[43] finds that the stripes align along the chain direction, reminiscent of LTT pinning. In a related 123 compound $(La_{1-x}Ca_x)(Ba_{1.75-x}La_{0.25+x})Cu_3O_y$, the La^{3+} at the Ba cite disrupts the chains, leading to an average tetragonal structure; in this case a plane buckling is observed, which is *largest at the doping of optimal superconducting* T_c.[44]

Bi2212. In $Bi_2Sr_2CaCu_2O_{8+\delta}$ (Bi2212), the orthorhombic ordering may be the cause[45] of the ''ghost'' Fermi surfaces observed in photoemission[46] and also couples strongly to the VHS. Most suggestively, it has recently been found that *the intensity of these ghost features peaks near optimal doping*.[47] This is close to the prediction of the VHS stripe model, in which the structural order should be maximal in the slightly overdoped regime, just when magnetic correlations disappear (termination of the stripe phase).

C. Competition and cooperation of the CDW's

In Sec. III, we will show that the molecular equivalent of the flux phase, the DJT state, arises from competition between the two other modes. In the cuprates, there is also evidence for a competition between the two types of CDW, which we briefly review here. In LSCO, both the breathing and the LTT modes show anomalous softening with doping. An interesting situation arises in YBCO. Pintschovius and Reichardt (p. 349 of Ref. 30) note that a special form of Van Hove nesting[39] can couple the dimpling and half-breathing phonon modes, leading to a large doping-dependent renormalization of the latter. Dimpling of the CuO_2 planes causes the VHS's to bifurcate (e.g., the X VHS splits along the Γ-X-Γ line). In turn, nesting between the bifurcated peaks leads to breathing mode softening along Γ-X and can lead to a period doubling instability. The exact nesting wave vector is controlled by the degree of VHS bifurcation, which in turn depends on the amount of dimpling. Thus, two phonon modes (here the dimpling and half-breathing modes) are strongly coupled by the VHS. A similar competition between breathing and octahedral tilt modes near a superconducting instability is found[48] in $Ba_{1-x}K_xBiO_3$; in this case the tilt modes are near the R point of the Brillouin zone, coupling to the three-dimensional VHS's.

Alternatively, since both kinds of phonons couple strongly to the VHS, softening of the breathing mode will repel the lower-frequency (LTT or dimpling mode) phonon and can drive that second mode soft. This strong mixing of the two modes can create a flux phase.

III. ELECTRON-PHONON COUPLING: FROM SQUARE MOLECULES TO CUPRATES

In this section, we show that the three electronic CDW modes (with or without their associated phonons) form a symmetry group and map the interaction to a molecular JT model. We demonstrate that the same degeneracy arises in both the molecular and lattice problems. In Sec. IV we apply these results to the cuprates, showing (Appendix B) how the phonons in LSCO fit into the scheme and calculating their coupling to electrons.

A. Pseudospin group

We begin with a purely theoretical description, based on the group theory of instability or spectrum generating algebras,[49] specialized to the VHS instability group,[5,50] of SO(8) symmetry. Within this group there is a triplet of CDW operators, which couple strongly to phonons. These operators are spanned by an SU(2) subalgebra which we call ''pseudospin.''

To specify the order parameters in terms of bilinear electronic operators, it is necessary to define these operators on *a larger unit cell*, containing a plaquette of four copper atoms,[15,50] replacing the copper (or Zhang-Rice singlet) wave functions by electronic states symmetrized on a single plaquette. These states $\psi_{+ijk}=(\psi_1+i\psi_2+j\psi_3+k\psi_4)/2$ have A_{1g} (ψ_{++++}), B_{2g} (ψ_{+--+}), and E_u $(\psi_{++--}, \psi_{+--+})$ symmetry. Introducing creation operators for the E_u doublet $a^\dagger_{\pm,\sigma}(\vec{r})=[\psi^\dagger_{E_{u1},\sigma}(\vec{r})\pm\psi^\dagger_{E_{u2},\sigma}(\vec{r})]/2$, the pseudospin can be written in terms of the Fourier transforms of these states. In the basis

$$\{B_\sigma(k)\}=\{a_{+,\sigma}(\vec{k}),a_{-,\sigma}(\vec{k})\}, \tag{1}$$

the explicit form of these matrices is

$$\tilde{O}_{BOW}=\frac{\tilde{\gamma}}{2}\tilde{T}_x, \tag{2}$$

$$\tilde{O}_{OAF}=\frac{\tilde{\gamma}}{2}\tilde{T}_y, \tag{3}$$

$$\tilde{O}_{CDW}=\tilde{T}_z, \tag{4}$$

where

$$\tilde{T}_x=\begin{pmatrix}0 & 1\\ 1 & 0\end{pmatrix}, \tag{5}$$

$$\tilde{T}_y=\begin{pmatrix}0 & -i\\ i & 0\end{pmatrix}, \tag{6}$$

$$\tilde{T}_z=\begin{pmatrix}1 & 0\\ 0 & -1\end{pmatrix}, \tag{7}$$

with $c_i=\cos k_i a$ and $\tilde{\gamma}=c_x-c_y$. The operators $\tilde{O}_{CDW}$, $\tilde{O}_{BOW}$, and $\tilde{O}_{OAF}$ transform exactly as a pseudospin near the VHS's ($c_x-c_y=\pm 2$), but not at a general point in the Brillouin zone. This same problem arises in SO(5),[51] and the Henley operator[52] was introduced to deal with it.

The electronic arrangements corresponding to these operators are illustrated in Fig. 1: O_{CDW} is a site CDW, with excess charge on the odd sites 1 and 3 and a deficit on the even sites 2 and 4; $\tilde{O}_{BOW}$ is a bond centered CDW (BOW), with excess charge on the 1-2 and 3-4 links and a deficit on the 1-4 and 2-3 bonds; while O_{OAF} is an orbital antiferromagnet, with an orbital current flowing clockwise, from $1\rightarrow 4\rightarrow 3\rightarrow 2$. In a three-band model, O_{CDW} would represent a Cu-based CDW and $\tilde{O}_{BOW}$ an O-based CDW. Note that the CDW mode is equivalent to the charge ordering found in $La_{2-x}Sr_xNiO_4$ for $x\sim 0.5$.[53] The orbital current operator[5] O_{OAF} is closely related to the flux phase.[1] In the flux phase, hopping is accompanied by an accumulation of a phase change by π on circulating a plaquette. For the plaquette of Fig. 1(c), this leads to a contribution to the Hamiltonian proportional to

$$H'=e^{i\pi/4}(a_2^\dagger a_1+a_3^\dagger a_2+a_4^\dagger a_3+a_1^\dagger a_4)+\text{H.c.}$$

$$=\frac{1}{\sqrt{2}}(a_2^\dagger a_1+a_3^\dagger a_2+a_4^\dagger a_3+a_1^\dagger a_4+\text{H.c.})-2\sqrt{2}T_y. \tag{8}$$

The first term in Eq. (8) corresponds to an (uninteresting) uniform hopping on the plaquette. Thus, up to this term, *the flux phase is equivalent to the orbital antiferromagnet* O_{OAF} (T_y).

While the instabilities are predominantly electronic, they are accompanied by lattice instabilities, as in the Peierls transition. In particular, the CDW couples to the oxygen breathing mode and the BOW couples naturally to a shear distortion; these are referenced to a single molecule in Fig. 2. The relation of this shear to the LTT tilting mode was clarified in Sec. II.

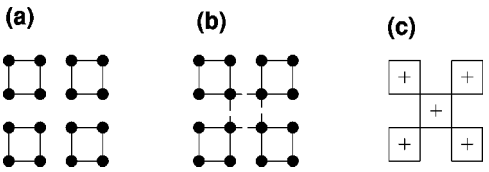

FIG. 3. Berryonic matter: two views of the lattice of square molecules, either as simple square (a) or as centered square with corner sharing molecules (b) compared with the flux phase (c), where the $+$'s indicate plaquettes with a $+\pi$ flux.

This pseudospin triplet is an exact condensed-matter analog to the molecular JT modes responsible for the DJT effects found in molecules. The enlarged unit cell associated with Eq. (1) provides a natural connection. Thus, we regard the CuO_2 planes as composed of a square array of Cu_4O_4 ''molecules'' bonded to each neighbor by a pair of oxygens. These molecules can be embedded into the lattice in two equivalent ways, as illustrated in Fig. 3. While it is simpler to analyze a square lattice of square molecules, as in Fig. 3(a), a more accurate representation is in terms of a ''centered square'' lattice as in Fig. 3(b). (Crystallographically, the centered square is not a primitive unit cell, but it is convenient for the present purposes.) The latter case has twice as many molecules, but they are corner sharing. The atoms (coppers and oxygens) in each molecule deform in the same way. For instance, Fig. 3(c) illustrates the flux phase, labeling each square plaquette which contains a $+\pi$ flux with a plus sign. When interpreted as in Fig. 3(b), the ground states have a twofold degeneracy, which is also found in the flux and CDW phases.

The above analysis resolves an old conundrum. Earlier calculations interpreted the LTT phase in terms of a Van Hove-Jahn-Teller (VHJT) effect,[15,29] where the electronic degeneracy is associated with the presence of two VHS's. This is puzzling, since JT effects usually have a simple molecular basis, but such a basis is not obvious in the present case. We now see that the VHJT effect on the conventional lattice is equivalent to a conventional JT effect on a supercell lattice. The resulting lattice constitutes a nearly exact realization of a Berryonic crystal—replacing the originally proposed[7] JT active triatomic molecules by square molecules.

The close connection between the JT and Van Hove viewpoints can be clarified by representing the CuO_2 plane electronic states in the supercell representation[15,50] defined above Eq. (1). Including nearest- (t) and next-nearest- (t') neighbor hopping, the kinetic energies are

$$E(A_{1g})=-2t-t',$$

$$E(E_u)=t',$$

$$E(B_{2g})=2t-t', \tag{9}$$

so at half filling, the A_{1g} level is filled and there are two electrons in the E_u levels. Optimal doping corresponds to one extra hole per plaquette, leaving one electron in the E_u levels, and a JT effect. The full band dispersion of the square lattice can be written as a superposition of these four states (Appendix I of Ref. 15). It is found that *all states near the*

VHS's are built up exclusively of E_u states. On the other hand, states near the nodal points have A_{1g} character. Note that this explicitly demonstrates that VHS instabilities persist down to ''lattices'' as small as a single 2×2 plaquette.

The above calculations are for the weak-coupling limit and are consistent with the charge ordered states found in Sec. IV. However, the analysis can be repeated in the strong-coupling limit. Thus, for an antiferromagnetic arrangement, the (mean-field) energies are $E(A_{1g})=E(B_{2g})=-t'-\sqrt{\bar{U}^2+4t^2}$, $E(E_u)=t'-\bar{U}$, with $\bar{U}\simeq U/2$. With parameters[54] $t\simeq325$ meV, $U/t\simeq6$, $t'/t\simeq-0.276$, and $J=4t^2/U$, $E(E_u)-E(A_{1g})\simeq2t'+J\simeq t/6>0$, so the first hole would again come from the E_u level, although all levels are close in energy. (Note that a smaller J would reverse the order of the levels but would still lead to an electronic degeneracy.) Thus, one can still have a JT instability in the strong-coupling limit, although its nature can be significantly modified. For a somewhat different example, see Ref. 55.

The present JT effect is significantly different from the conventional JT effect of a CuO_6 octahedron, which involves the electronic (pseudo)degeneracy associated with the Cu d_{z^2} and $d_{x^2-y^2}$ orbitals. Many earlier studies (e.g., Refs. 13 and 56) have proposed that this (pseudo-)JT effect plays an important role in cuprate physics. The present model works even if the d_{z^2} orbitals are completely uncoupled (although a residual coupling could enhance the present effects). The model is closer to the large polaron limit,[57,58] but with a particular choice of polaronic coupling dictated by the underlying SO(8) group structure.[50]

B. Molecular Jahn-Teller effect

As a preliminary to studying the VHJT effect on a lattice, we first look at the molecular analog, a Cu_4O_4 molecule with square planar symmetry, D_{4h}, which corresponds to the $E\otimes(b_1+b_2)$ JT problem.[11,59,60] This molecule can display a DJT effect which bears a striking resemblance to the flux phase. Figure 2 displays the relevant B_1 and B_2 distortions, assuming predominantly oxygen vibrations. The B_2 distortion is the oxygen breathing mode, while the B_1 has the form of the shear wave associated with the LTT instability.

The JT energy can be written $E_{JT}^{(i)}=V_i^2/(2M\omega_i^2)$, where V_i is the electron-phonon coupling and M is the ionic mass. In terms of E_{JT}, there are three classes of solution:

(i) $E_{JT}^{(1)}\neq E_{JT}^{(2)}$,

(ii) $E_{JT}^{(1)}=E_{JT}^{(2)}$ but $\omega_1\neq\omega_2$,

(iii) $E_{JT}^{(1)}=E_{JT}^{(2)}$ and $\omega_1=\omega_2$.

For case (i) the lowest-energy state consists of a static JT distortion of the mode with larger JT energy only. This simple case may apply to the cuprates: it has long been a puzzle why the oxygen breathing modes do not display the large softening expected[27] near (π,π). On the other hand, the LTT mode is quite soft and nearly unstable. This would follow if $E_{JT}^{(1)}>E_{JT}^{(2)}$. The results of Sec. IV are consistent with this possibility. However, formally the special cases (ii) and (iii) are more interesting, allowing dynamic solutions which are closely related to the flux phase.

Case (iii) reduces exactly to the well-known $E\otimes e$ problem of the triatomic molecule,[8,9,61] and *the electronic wave function is double valued*: when the molecular motion undergoes a 2π rotation, the electronic wave function picks up an extra factor of π, the Berry phase.[61,62] However, in the cuprates the phonon frequencies are very different (Appendix B), so case (iii) does not apply. Nevertheless, condition (ii) (weak degeneracy) may hold approximately in the cuprates, and it is known that inclusion of quadratic vibronic coupling enhances the range of case-(ii) degeneracy.[63] This special case has recently been analyzed:[60] the DJT effect with π Berry phase is preserved, although the classical motion may be *chaotic*.

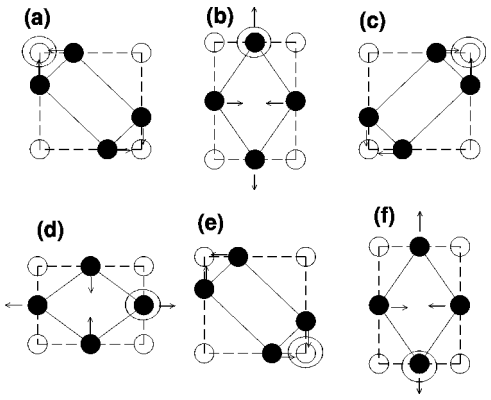

FIG. 4. Dynamic JT rotation mixing B_1 and B_2 modes of O_4. Large open circle represents one hole. Each time step (a)–(f) represents one-quarter of a cycle of molecular rotation, so in frame (e) the molecules have completed one cycle of rotation with respect to frame (a), while the hole has completed only half a rotation.

The origin of the wave function sign change is explained in Fig. 4. As each oxygen atom rotates about its undistorted position, the hole (large circle; a second hole is in the symmetric position) rotates about a different origin, the center of the square. When the individual atoms complete one full rotation, the hole has only completed half of a rotation, just as in the triangular molecule.[8] When the atoms complete a second rotation, the hole returns to its initial position for the first time. In analogy with the triatomic molecule, the electronic wave function can be kept single valued by multiplying it by a phase factor $e^{i\theta/2}$, where θ is the electronic rotation angle. [Parenthetically, it can be seen from the above figure that, in addition to the phonon modes listed in Sec. II B, the Cu $(\pi,0,0)$ half-breathing mode, by changing the Cu-O distance, would couple to the BOW mode.]

Thus, the DJT effect with anomalous Berry phase exists for a square molecule; while this involves some ''fine-tuning,'' the matching requirement may be relaxed by quadratic vibronic coupling.[63] In the following subsection, we will see that a similar accidental degeneracy exists for the lattice problem, and it is known that the structural transitions in LSCO are strongly nonlinear.[14,64]

C. Extension to the lattice

In this subsection we formally derive the condition for the degenerate case (ii) to occur when the $E\otimes(b_1+b_2)$ problem is extended to the lattice. We follow the notation of Ref. 65, treating each plaquette as a lattice site, labeled $\vec{l}$, which

therefore has three relevant electronic modes $\tau_i(\vec{l})$, $i=1,2,3$. Following standard JT practice, we will only include the two real modes $i=1,2$ [corresponding to Eqs. (2) and (4)] in the Hamiltonian. The JT coupling becomes

$$H_{JT}=\sum_{i=1,2} H_{JT,i}, \tag{10}$$

$$H_{JT,i}=-\eta_i e_i \sum_{\vec{l}} \tau_i(\vec{l}) - \sum_{\vec{q}} \sum_{m} v_i^m(\vec{q}) Q_i^m(\vec{q}) \tau_i(-\vec{q}), \tag{11}$$

where the corresponding phonon modes are $Q_i^m(\vec{l})$ [with Fourier transform $Q_i^m(\vec{q})$], the m sum is over different phonon branches of a given symmetry, v_i^m is the linear electron-phonon coupling constant, and we include coupling to the elastic strains, with e_i and η_i the strain component and its coupling to τ_i. If the phonon Hamiltonian is written

$$H_{ph}=\frac{1}{2}\sum_{i,m,\vec{q}} M\omega_{i,m}^2 Q_i^m(\vec{q}) Q_i^m(-\vec{q}), \tag{12}$$

with M an appropriate ionic mass, then the linear coupling to Q_i can be replaced by an effective electron-electron coupling by the displaced oscillator transformation:

$$\hat{Q}_i^m(\vec{q})=Q_i^m(\vec{q})+\frac{v_i^m(-\vec{q})\tau_i(\vec{q})}{M\omega_{i,m}^2}. \tag{13}$$

This transformation approximately decouples the phonons, leaving an interaction

$$H_{int}=-\sum_{i,\vec{l}} \eta_i e_i \tau_i(\vec{l}) - \frac{1}{2}\sum_{i,\vec{q}} J_i(\vec{q})\tau_i(\vec{q})\tau_i(-\vec{q}), \tag{14}$$

with $J_i(\vec{q})=\Sigma_m K_i^m(\vec{q})$,

$$K_i^m(\vec{q})=\frac{v_i^m(\vec{q})v_i^m(-\vec{q})}{M\omega_{im}^2(-\vec{q})}. \tag{15}$$

This decoupling is only approximate, since the $\hat{Q}$'s depend on the τ's, so that they do not obey canonical commutation relations. It will, however, be adequate for the present purposes. At the mean-field level,

$$\eta_i\langle e_i\rangle=\mu_i\langle\tau_i\rangle, \tag{16}$$

with $\mu_i=N\eta_i^2/2c_i^0$ and c_i^0 the bare elastic constant. Letting[65]

$$\lambda_i=\mu_i+\sum_m \left(K_i^m(0)-\frac{1}{N}\sum_{\vec{q}} K_i^m(\vec{q})\right) \tag{17}$$

and assuming only one Δ_i is nonvanishing, the gap equations are

$$\Delta_i=\lambda_i\langle\tau_i\rangle, \tag{18}$$

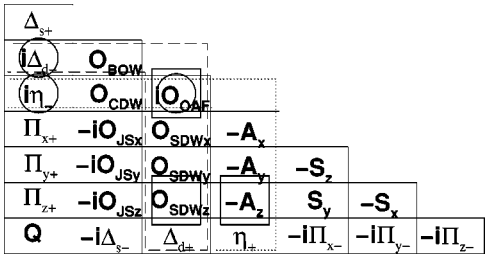

FIG. 5. SO(8) operator algebra, illustrating the representation of the algebra in terms of antisymmetric matrices. Dashed and dotted boxes illustrate those elements which do not commute with the flux phase operator O_{JC}. Circled and boxed elements represent isospin triplets involving O_{JC}. (The four other triplets are not accentuated.)

$$\langle\tau_i\rangle=-\sum_{\vec{k}} \Delta_i \frac{f(E_+(\vec{k}))-f(E_-(\vec{k}))}{E_+(\vec{k})-E_-(\vec{k})}, \tag{19}$$

with $E_\pm$ the energy eigenvalues and $f(E)$ the Fermi function. If $\lambda_1\neq\lambda_2$, only the mode with larger λ_i has a nonzero expectation value, although both modes can soften above the transition temperature. However, when

$$\lambda_1=\lambda_2, \tag{20}$$

then $\Delta_1=\Delta\cos\theta_0$, $\Delta_2=\Delta\sin\theta_0$, with θ_0 arbitrary. Equation (20) is the generalized version of condition (ii).

D. Operator algebra cookbook: Six ways to prepare a flux phase

The *dynamic JT effect* follows directly from the above operator algebra, Eqs. (2)–(7). Note that the commutator of any two T_i's is the third T_i. This has important consequences for competing orders: if *any two* of the operators have a finite expectation value, then *the third operator must also be present*. (No restrictions are placed on situations where only one operator has a finite expectation value.) In the usual development of the dynamic JT effect, this group theoretical aspect is lost, as the dynamic, T_y operator is treated on a very different footing from the other two: the ''static'' (real) electronic operators appear in the Hamiltonian, explicitly coupled to static distortions; the ''dynamic'' component is then generated dynamically from the degeneracy of the first two modes. In reality, this is a quite general operator property, extending to every subgroup of the SO(8) or SU(8) operator algebras.[50,49] Perhaps the best known case is competing antiferromagnetic and *d*-wave superconducting orders: the simultaneous presence of both orders requires the presence of a third component, the π phase.[66,51] Murakami[67] has discussed several related examples.

We illustrate the advantages of the operator algebra approach, by demonstrating all the pairs of competing operators which will generate a flux phase. This amounts to all the SU(2) subalgebras of the covering algebra—in the present case, an SO(8) algebra.[50] Figure 5 shows the representation of SO(8) in terms of antisymmetric 8×8 matrices. The operators are defined in Ref. 50. In the matrix representation, each operator is represented by an antisymmetric matrix with two nonzero elements: a 1 in the position below the diagonal corresponding to the symbol in Fig. 5 and a -1 in the corresponding position above the diagonal (since the diagonal

elements are zeros, they are not displayed). For example, elements which do not commute with the flux phase operator O_{JC} must lie in the same column or row of the figure; since only elements below the diagonal are illustrated, these correspond to the dashed and dotted boxes, respectively. Choosing any element from the same column (dashed box)—say Δ_{d-}—the commutator of that element with O_{JC} is given by the element in the dotted box which shares the same row with the first element. Thus, η_- goes with Δ_{d-} (circles in Fig. 5), CDW with BOW, etc. By following this procedure, all of the isospin triplets discussed by Murakami[67] are readily generated.

Each set of three elements so generated forms a closed SU(2) algebra[68] and leads to a form of generalized DJT effect. Unfortunately, in the present instance, most of the other operators are even more obscure than the flux phase. The η operator comes up in the positive-U Hubbard model. There the ground state involves competing CDW O_{CDW} and s-wave superconducting operators (where $\Delta_{s\pm}=\Delta_s\pm\Delta_s^\dagger$), and when both operators are present, an η phase must appear—see the representation matrix. In principle, then, if one could generate simultaneous d-wave superconductivity and η phase, a flux phase would also appear. The $\vec{A}$ phase has not been previously discussed. It appears to be a form of d-wave ferromagnet. For example, on a square lattice the $\vec{k}$-space representation of A_z is

$$A_z=\sum_{\vec{k}}\frac{\tilde{\gamma}}{2}(a^\dagger_{\vec{k},\uparrow}a_{\vec{k},\uparrow}-a^\dagger_{\vec{k},\downarrow}a_{\vec{k},\downarrow}). \tag{21}$$

However, when antiferromagnetic (AFM) and flux phases are simultaneously present, the $\vec{A}$ phase will be spontaneously generated.

IV. APPLICATION TO THE CUPRATES

A. Electron-electron coupling

In Sec. III C, a formal definition was given for the JT problem on a lattice of plaquettes. Here it is convenient to redefine the operators on the square lattice of the cuprates and demonstrate that they are equivalent to the earlier set of operators. We begin with a purely electronic model of the CDW's; it will turn out (Sec. IV B) that the electron-electron interaction actually dominates the electron-phonon coupling in the cuprates. While the exact mode coupling is not known, a simple extended Hubbard model is convenient to analyze, since the nearest-neighbor Coulomb interaction V contributes to all three components of pseudospin, Eqs. (2)–(4). The resulting mean-field interactions are[55]

$$\begin{aligned}V\sum_{\langle i,j\rangle,\sigma,\sigma'}n_{i,\sigma}n_{j,\sigma'}=&-8V\langle T_z\rangle\sum_{\vec{k},\sigma}c^\dagger_{\vec{k}+\vec{Q},\sigma}c_{\vec{k},\sigma}\\&-4V\langle T_x\rangle\sum_{\vec{k},\sigma}\tilde{\gamma}_k c^\dagger_{\vec{k},\sigma}c_{\vec{k},\sigma}\\&+4V\langle T_y\rangle i\sum_{\vec{k},\sigma}\tilde{\gamma}_k c^\dagger_{\vec{k}+\vec{Q},\sigma}c_{\vec{k},\sigma}\\&+4NV(\langle T_z\rangle^2+\langle T\rangle^2),\end{aligned} \tag{22}$$

where $\langle T\rangle^2=\langle T_x\rangle^2+\langle T_y\rangle^2+\langle T_z\rangle^2$ $\tilde{\gamma}_k=(c_x-c_y)/2$. The gap equations are

$$\sum_\sigma\langle c^\dagger_{i,\sigma}c_{i,\sigma}\rangle=1-x+2(-1)^{\vec{r}_i}\langle T_z\rangle, \tag{23}$$

$$\langle c^\dagger_{i,\sigma}c_{i+\hat{x},\sigma}\rangle-\langle c^\dagger_{i,\sigma}c_{i+\hat{y},\sigma}\rangle=2(\langle T_x\rangle+i(-1)^{\vec{r}_i}\langle T_y\rangle). \tag{24}$$

The notation $\langle T_i\rangle$ is introduced to stress the close connection with matrix elements of the $\tilde{T}_i$ operators in Eqs. (5)–(7) above. Below, it will be convenient to renormalize these parameters: $R_{x0}=-4V\langle T_x\rangle$, $R_{y0}=-4V\langle T_y\rangle$, and $R_{z0}=-8V\langle T_z\rangle$.

The CDW modes break the degeneracy of the bipartite lattice. We therefore define the fourier transform of the creation operator as a matrix:

$$a_{\vec{R},\vec{q}}=a^0_{\vec{R}}e^{i\vec{q}\cdot\vec{R}}. \tag{25}$$

Writing $\vec{R}=a(i\hat{x}+j\hat{y})$, where $\hat{x}$ and $\hat{y}$ are unit vectors and i, j are integers, then

$$a^0_{\vec{R}}=\begin{cases}a_o & \text{if } i+j \text{ is even,}\\ a_e & \text{if } i+j \text{ is odd.}\end{cases} \tag{26}$$

The Hamiltonian is then a matrix in a_o and a_e or, alternatively, in $a_\pm=(a_o\pm a_e)/\sqrt{2}$. The latter choice is equivalent to restricting the $\vec{q}$ sums to the ''magnetic'' Brillouin zone, with $\epsilon_{\vec{k},+}=\epsilon_{\vec{k}}$, $\epsilon_{\vec{k},-}=\epsilon_{\vec{k}+\vec{Q}}$. Here, we expand in a_o and a_e. In this case, the electronic part of the Hamiltonian can be written $H=H_{el}+H_1$ where the electronic kinetic energy is

$$H_{el}=\begin{pmatrix}E_1 & E_0\\ E_0 & E_1\end{pmatrix}, \tag{27}$$

with $E_0=-2t(c_x+c_y)$, $E_1=-4t'c_xc_y$, and t (t') is the (next-)nearest-neighbor hopping parameter. At mean field, the effects of both V [Eq. (22)] and the on-site Coulomb interaction U can be included, leading to the Hamiltonian matrix

$$H_{el}+H_1=\begin{pmatrix}R_{z\sigma}+E_1 & E_0+R_x+iR_y\\ E_0+R_x-iR_y & -R_{z,\sigma}+E_1\end{pmatrix}, \tag{28}$$

with eigenvalues

$$E_{\pm,\sigma}=E_1\pm\sqrt{R^2+E_0^2+2R_xE_0}, \tag{29}$$

where $R^2=R_x^2+R_y^2+R_{z,\sigma}^2$, Fig. 6. In Eqs. (28) and (29), we take $R_x=R_{x0}\tilde{\gamma}$, $R_y=R_{y0}\tilde{\gamma}$, and $R_{z,\sigma}=R_{z0}+\sigma Um_z$, where the R_{i0}'s are defined below Eq. (24), $\sigma=\pm1$ is the spin, and m_z is the average magnetization per site in the antiferromagnetic phase induced by U. Parameter values are given in Sec. III A, and it is estimated[69] that $V\simeq0.2$–0.3 eV. Note that R_x simply renormalizes t to have unequal values in the x and y directions.[33,35,36]

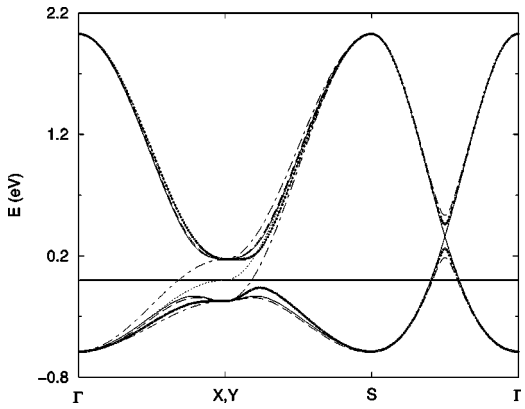

FIG. 6. Energy dispersion in the presence of pseudospin ordering, Eq. (29), for $t=0.326$ eV, $t'=-0.276t$, and $R_{x0}=R_{y0}=R_{z0}=0.1$ eV (short dashed line), or $R_{i0}=0.1732$ eV and the other two R's=0, for $i=x$ (dot-dashed line), y (solid line), or z (long dashed line), or all R_i's=0 (dotted line).

By comparing Eq. (28) with Eqs. (2)–(7), the essential equivalence of the lattice modes to the single plaquette modes is clearly demonstrated. The conventional[1] flux phase dispersion is recovered from Eq. (29) for the special choice of parameters: $t'=R_{x0}=R_{z,\sigma}=0$ and $R_{y0}=2t$ [compare Eq. (8)]. The extension to the lattice involves a number of minor differences. First, while the term involving T_y is generated dynamically in the molecular problem, here a term in R_y appears explicitly. On a single plaquette, the three solutions are degenerate (the eigenvalues depend only on R, and not on the individual R_i's), but intercell hopping and k-dependent coupling lead to slight dependence of the dispersion on the individual R_{i0}'s. The solutions remain degenerate at the VHS, for equal R_{i0}'s.

Introducing the polarization

$$\Pi_{\vec{k},\sigma}=-\frac{f(E_{+,\sigma})-f(E_{-,\sigma})}{E_{+,\sigma}-E_{-,\sigma}}, \tag{30}$$

the gap equations can be written

$$\sum_{\sigma}\int_{\vec{k}}\Pi_{\vec{k},\sigma}\Lambda_i=1, \tag{31}$$

for i including all the nonvanishing gap contributions. The most general case has all four gap parameters R_{x0},R_{y0},R_{z0},m_z nonvanishing, with corresponding $\Lambda_1=\lambda_1(\tilde{\gamma}+E_0/R_{x0})\tilde{\gamma}$, $\Lambda_2=\lambda_2\tilde{\gamma}^2$, $\Lambda_3=\lambda_3(R_{z,\sigma}/R_{z0})$, and $\Lambda_4=\lambda_4(1+\sigma R_{z0}/Um_z)$. For the extended Hubbard model, the λ's are[55] $\lambda_1=\lambda_2=8V$, $\lambda_3=16V-2U$, and $\lambda_4=2U$. (In the areas of overlap, these gap equations agree with those found by Nayak.[70] In contrast, a strong-coupling calculation[71] has suggested that only an attractive near-neighbor coupling would stabilize the flux phase.)

In the absence of on-site U, the near-neighbor interaction V favors the CDW, R_z. The energy lowering is exactly twice that of the other components, the factor of 2 arising from spin (since the x and y terms involve hopping, only terms with the same spin on both neighbors contribute; the z term has no such limitation). This is counteracted by strong-coupling effects, since the CDW involves an imbalance of Cu site occupancies. Approximating $V=t$, $U=6t$, $8V>16V-2U$, favoring the flux and shear phases. Because the couplings are not symmetrical [Eq. (29)], these modes have slightly different gaps, $R_{x0}=340$ meV, $R_{y0}=320$ meV, and $R_{z0}=8.4$ meV. However, $2U>8V$, so in a purely electronic model the antiferromagnetic phase dominates, both at half filling and in the doped case. In the following subsections, it will be shown that electron-phonon coupling can reverse this situation in the doped cuprates and also brings the CDW energy closer to that of the other phases.

B. Electron-phonon coupling

In Appendix B, a general model is developed for evaluating the electron-phonon coupling due to various bond stretching and bending modes of copper and oxygen vibration. First, the changes in the site energies and hopping parameter of a three-band model are evaluated (Appendix B 1), then the results are reduced to a one-band model (Appendix B 2), which can be combined with the electron-electron interaction terms evaluated above. While a number of phonon modes are analyzed, the electronic modes are dominant, so it is sufficient to limit the discussion to the three modes of primary interest. Appendix B also introduces a simple model of phononic flux phases—the dynamic phonon modes which directly couple to the flux phase.

The gap equations follow from minimizing the mean-field free energy

$$F=\sum_{k,i=\pm}E_i f(E_i)-TS+Nf_0\equiv F_1+Nf_0, \tag{32}$$

where S is the entropy, N the total number of electrons, and

$$f_0=\frac{R_{x0}^2+R_{y0}^2}{4V}+\frac{R_{z0}^2}{8V-U}+\sum_{i=1,3}A_i\left(\frac{\delta u_i}{a}\right)^2+U\left(m_q^2+\frac{x^2}{4}\right), \tag{33}$$

where the phonon contribution (terms in A_i) is evaluated in Appendix B, Table III. The E_i are solutions of Eq. (29) with phonon coupling included by the substitution $R_{i0}\rightarrow\overline{R}_{i0}=R_{i0}+R_{iph}$, $i=x,y,z$. [N.B. The original R_{i0}'s are retained in f_0, Eq. (33).] This simple correction comes about because in the one-band model, the linear electron-phonon coupling has exactly the same form as the V electron-electron term in Eq. (28). This also simplifies the evaluation of the phonon terms R_{iph}. The electronic terms are found from $\partial F/\partial R_{i0}=0$, while the phonon terms satisfy $R_{iph}=\eta_i R_{i0}$, with coupling parameters η_i evaluated in Appendix B 2, Eqs. (B9) and (B10). Inserting the numerical values from Table III, we estimate

$$\eta_z\simeq 0.88, \tag{34}$$

$$\eta_x\simeq 0.137, \tag{35}$$

$$\eta_y\simeq 0.1. \tag{36}$$

The estimation of these parameters is less secure than that of the electronic parameters. To allow for this uncertainty, we

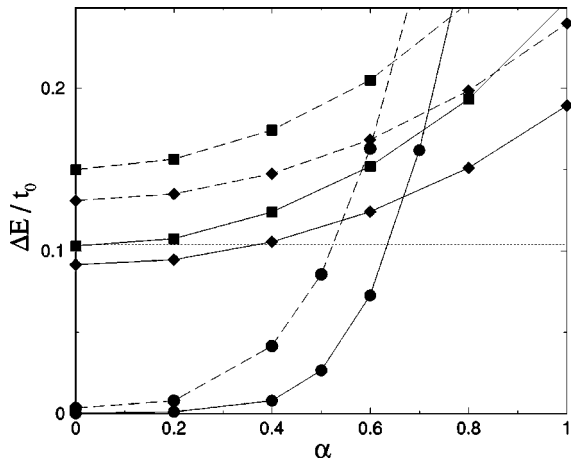

FIG. 7. Binding energy of various modes: site-CDW (circles), bond-CDW (squares), and flux phase (diamonds), for $\beta_{loc}=0$ (solid lines) or 0.1 (dashed lines); horizontal dotted line = energy of doped antiferromagnetic phase. For all curves $x=0.25$.

introduce scaling parameters α_i, via $\eta_i=\eta_i^0\alpha_i^2$, where we expect $\alpha_z=\alpha_d$, $\alpha_x=\alpha_y=\alpha_t$ (Appendix B 2). In the above estimates, we took $\alpha_d=0.5$, $\alpha_t=1$. Below, we will explore how the coupling changes as the α's are varied.

From the above results, we see (1) there is substantial phonon coupling, but the transitions appear to be predominantly electronically driven. (2) The largest correction is for the CDW mode, although the correction is not large enough to make the CDW as unstable as the other two modes (if α_d were twice as large as estimated, all three modes would be approximately degenerate). (3) Near half filling the corrections are not large enough to make any of the structural anomalies competitive with the AFM instability. This result is consistent with the finding of Hsu *et al.*:[72] that the flux phase is unstable against magnetic order near half filling and, with experiment, that the ground state at half filling has AFM order. (4) At finite doping, the added electron-phonon coupling is strong enough to make the BOW the ground state (Fig. 7, below). In the following subsection we note that a particular form of correlated hopping can substantially enhance the stability of the CDW's.

In addition to the three modes discussed above, Appendix B also analyzes the half-breathing mode and finds that it softens considerably more with doping than the full (π,π) breathing mode, Fig. 11, in good agreement with experiment. The reason is subtle: the full breathing mode has the strongest coupling to electrons, but by tending to open a gap on the whole Fermi surface, it has its largest effect *at half filling* and so tends to harden with doping. The weaker coupling of the half-breathing mode is optimized at the VHS. Below, it is seen that strong coupling suppresses the breathing mode coupling at exactly half filling, but its effect still peaks at a considerably lower doping than for the other modes.

C. Unconventional coupling associated with O^{2-}

The O^{2-} ion is known to be inherently unstable, being stabilized in a solid by the Madelung potential of surrounding ions. It has been suggested that this near instability is a driving force in ferroelectric transitions[73] in perovskites and in cuprate superconductivity.[74] One manifestation of this near instability is the large change in ionic radius on doping O^{2-} to O^{-}.[33] While this anomaly should affect the electronic properties in a number of ways, we will here explore only one aspect, a correlated hopping.

When a hole is *localized* on a single oxygen, the shrinkage of its radius allows the adjacent coppers to approach much more closely. This would enhance the corresponding hopping probability t except that the presence of the hole inhibits other holes from hopping to the same site. If, however, the first hole hops away, it will take the local lattice some time to relax back, and in that interval there will be an enhanced probability of another hole hopping onto the oxygen. [N.B. The hopping is the usual hopping of a hole onto an unoccupied oxygen O^{2-}; the difference is that the bond lengths to the surrounding coppers are (instantaneously) anomalously short, due to the prior occupation of the oxygen by a hole.] In a one-band model, this would correspond to correlated hopping between adjacent Zhang-Rice singlets or, effectively, between adjacent coppers. This hopping adds a term

$$H_{c.h.}=-t_{c1}\sum_{\langle i,j\rangle,\langle i',j\rangle,i\neq i'} c_{i\sigma}^{\dagger}c_{j\sigma}c_{j\sigma'}^{\dagger}c_{i'\sigma'} \qquad (37)$$

to the Hamiltonian. Such a term has been considered by Nayak;[70] more generally, Hirsch and Marsiglio[75] noted that the large difference in ionic size between ions with different valences should lead to a form of correlated hopping. This term contributes $96t_{c1}$ to all three coupling parameters λ_i, $i=1,2,3$. From the present considerations, a value $t_{c1}=-2x\beta_{loc}\beta t\,\delta u_0/a\propto xt$ can be estimated, where $\delta u_0\sim -0.3$ Å is the shrinkage in radius[33] on going from O^{2-} to O^{-}. The factor x arises because holes only move preferentially onto the oxygens for doping beyond half filling, $x>0$, while $\beta_{loc}\leqslant 1$ is a parameter introduced to describe the degree of localization of the hole on a single oxygen—predominantly due to polaronic effects. This factor is related to the delicate issue of the crossover from ionic to covalent behavior: $\beta_{loc}=1$ corresponds to the ionic limit. The t_{c1} correction is so large that even a significantly covalent correction $\beta_{loc}<1$ would allow the structural distortions to overcome the AFM state—but only for $x>0$.

D. Numerical results

Here we describe our numerical results, solving the gap equations which follow from Eq. (32). Figure 7 plots the self-consistent condensation energy as the phonon coupling is gradually turned on by varying the α factors ($\eta_i\propto\alpha_i^2$) from zero (no phonon coupling) to 1, covering the expected range of coupling. We study the coupling near the VHS, $x=0.25$. For weak phonon coupling, the CDW has the weakest coupling, due to the on-site Coulomb repulsion. However, it has the strongest intrinsic coupling to phonons, so as α_d is increased, it grows fastest and can actually cross the other modes. The dotted line is the energy of the simple doped antiferromagnet (also at $x=0.25$). It can be seen that for

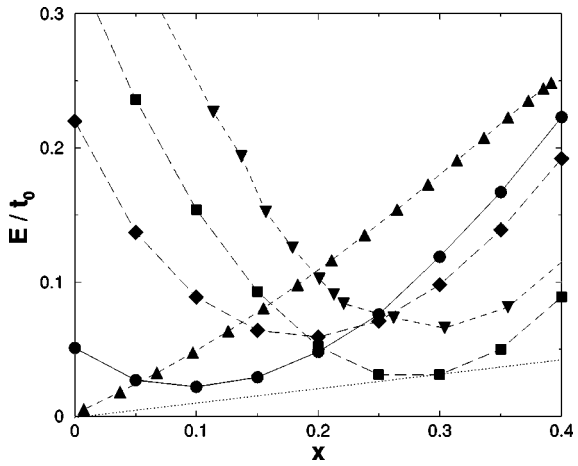

FIG. 8. Doping dependence of binding energies of phonon modes: site-CDW (circles), bond-CDW (squares), and flux phase (diamonds), assuming all mode α's=0.6, and $\beta_{loc}=0.1(x/0.25)$. Also shown is the doped antiferromagnet (triangles) and ferromagnet (inverted triangles) (Ref. 55). The dotted line is the tangent construction for phase separation. For convenience in viewing, an energy shift $\delta E=2.1(1-x)t_0$ has been added to all curves.

reasonable phonon coupling, the BOW is the ground state. The dashed lines show that even moderate correlated hopping ($\beta_{loc}=0.1$) significantly enhances the binding energies and shifts the degeneracy points of the CDW with the other modes to lower values of α.

In Fig. 8 the doping dependence of the binding energies is illustrated for a representative $\alpha_i=0.6$ $(i=d,t)$, compared to that of the doped antiferromagnet and ferromagnet.[55] All three CDW modes have a parabolic binding energy vs doping: for the bond-CDW and flux modes, the energy minima are near the VHS doping, while the site-CDW minimum is shifted to lower doping by the frustration effect discussed above (the minimum is no longer at $x=0$, due to the strong correlation effect). The results can be interpreted in two ways: (1) if phase separation could be inhibited, there would be a crossover from CDW to shear-mode order near $x\sim 0.21$, close to the VHS. Remarkably, all three CDW curves approximately converge (weak JT degeneracy) at this point.

(2) However, this crossover point is not directly observable. A by-now-familiar[17,76] Van Hove–induced phase separation arises between the antiferromagnetic insulator at half filling and *any* of the CDW modes. For the present parameter values, the lowest-energy state involves the BOW at $x\sim 0.27$. Note in particular that the BOW is more stable than the ferromagnetic phase.[55] At this time we have not made a detailed study of the parameter dependence of these results, but the present result—BOW most stable—seems to be appropriate for the cuprates. In particular, (a) α_d should probably be less than α_t, and (b) while our estimate for V may be a little large, t_{c1} is probably too small, so V can be reduced and t_{c1} increased to keep a fixed coupling to the shear mode. Both of these corrections would act to further weaken the site-CDW. The results are quite intriguing. For a reasonable estimate of the parameters there is phase separation between the antiferromagnetic insulator and a paramagnetic state associated with LTT-like distortions, while the CDW and flux-phase states are close in energy. Appendix A shows that this is generally consistent with experiment.

(3) Where they overlap, our results are in good agreement with the numerical calculations of Yonemitsu *et al.*[77] For instance, Fig. 8 shows that there would be a phase separation between the AFM and CDW phases, consistent with their dielectric polarons. Moreover, our finding that the ferromagnetic phase is metastable in the presence of bond CDW's is consistent with their finding of a crossover from magnetic to dielectric polarons in the low-doping regime. However, in their work V was not included, so their phonon anomalies are of the breathing-mode type, with neither shear-mode coupling nor evidence of DJT-like mode competition.

The present approach of turning on the electron-phonon interaction last (Fig. 7) makes the resulting near degeneracy seem rather accidental. It is more natural to reexpress the result: for *both* electron-electron (V) and electron-phonon coupling, the flux and BOW phases are nearly degenerate, while the site-CDW is more strongly coupled. However, the on-site Coulomb repulsion opposes site-CDW formation, making the three modes nearly degenerate in energy.

V. DISCUSSION: FUTURE DIRECTIONS

The present paper establishes the framework for analyzing CDW's in the cuprates and Berryonic matter in a number of related materials. Clearly much work remains to be done. This includes the following.

(1) From the associated susceptibilities the modifications to the electronic dispersion can be calculated and compared with the kink[78–80,18] seen in photoemission. While phononic contributions appear to be important,[18] Valla[80] has noted that the linear frequency dependence of the imaginary self-energy extends to much too high frequencies to be solely due to strong electron-phonon coupling. This is consistent with the present results: that the CDW has a strong electron-electron component. Hence, both components will be important in interpreting the photoemission dispersion, with proximity to a VHS providing a marginal Fermi liquid-like[81] background and phonon coupling the kink in the dispersion.

(2) The manner in which the y component couples to the Hamiltonian is markedly different in the molecular and lattice versions of the theory: in the molecular version, the direct electron-phonon coupling is to the x and z components (B_1 and B_2 modes), with the DJT term generated dynamically—from the phonon kinetic energy term. In the lattice, the flux-phase term arises directly from electron-electron coupling via V, and corresponding terms are allowed in the Hartree-Fock expansion of the electron-phonon coupling. It remains to be seen what role phonon kinetic energy plays in the lattice problem. (One effect will presumably be the kink in the electronic dispersion when $E=\hbar\omega_{ph}$.)

(3) Fluctuations of the CDW's (or of the stripes) should appear as new low-frequency (or pinned) phason modes.[60] It is possible that such modes have been observed in microwave measurements.[82]

(4) It will be important to provide detailed calculations showing how the shear mode couples to the various bond bending modes in the different cuprates. A related issue is

whether there are tilt distortions in the flux phase. (If so, then experimental evidence for local LTT order could really be associated with the flux phase.)

(5) One puzzling feature is the role of the LTO phase. Near optimal doping it would seem to be predominantly associated with local LTT order, but it seems to be a uniform phase near half filling. In principle, its presence could be accidental, particularly since it is only present in LSCO, but it does provide an easy axis for orienting the spins and, hence, may be involved in the stripe crossover from vertical to diagonal. [Also, the pseudogap seems to follow $T_{pg}(x) = 2T_{LTO}$.[29]]

(6) A very similar model should apply to the nickelates, and extensions can be made to other forms of Berryonic matter.

(7) There remains the problem of the competition of density-wave order with superconductivity.

(8) The detailed hole doping dependence must be worked out, including stripes and the effects of magnetic fluctuations.

This last point—or more precisely the role of strong correlations—should be elaborated on. The present calculations include the on-site Hubbard U, but from a Hartree-Fock spin-density-wave (SDW) approach. It is not clear how realistic this is, and if the correct ground state is very different from the one assumed here (Fermi liquid like on the charged stripes and domains), that would cast doubt on the current models of electron-phonon coupling. In our defense, we note the following points: (a) this model can explain the dispersion of the insulating oxycloride at half filling as a lower Hubbard band.[54] (b) For hole doping, the model correctly predicts the instability towards nanoscale phase separation.[55] (c) For electron doping, it is predicted that such phase separation is absent,[83,55] and the model has recently been shown to predict a detailed doping dependence of the collapse of the Mott gap[84] in NCCO in excellent agreement with experiment.[85] (d) The effective Hubbard U is found to be doping dependent: while even at half filling, U is smaller than the bandwidth $W=8t$, with doping U decreases to less than $W/2$, suggesting that the SDW approach should work, at least in the doped material. (e) The current calculations find that at half filling electron-phonon coupling and CDW effects are indeed suppressed, but they reappear at finite doping. The reduction in U noted above was not accounted for in the present calculations, but would clearly enhance this trend. Thus we feel that the present results will not significantly change with a more accurate treatment of correlation effects and that electron-phonon coupling plays a significant role in the doped cuprates.

VI. CONCLUSIONS

This results of this paper have bearings on four separate issues. First, on a purely formal level, the paper presents an alternative approach to the DJT effect in solids, revealing previously unsuspected analogies between flux phases and Berryonic matter. Second, the approach is applied to the cuprates, which are an *a priori* unlikely candidate for these DJT effects. Nevertheless, a ''hidden'' JT degeneracy is found, and a numerical estimate suggests that the cuprates are close to the weak-degeneracy point of a square molecule, which should enhance the possibility of a dynamic flux phase. These calculations can be considered a generalization of the results of Yonemitsu *et al.*,[77] by (a) reducing the problem to a one-band model, (b) providing a mean-field underpinning for the numerical calculations of local electronic phase separation, and (c), most importantly, including a nearest-neighbor Coulomb repulsion which enhances the scope of CDW-like instabilities, producing the dominant coupling to the shear-mode and flux phases. Third, the paper explores the relative strength of different CDW-like distortions in the cuprates and suggests an explanation for strong coupling to the LTT and half-breathing modes. The role of these distortions in stabilizing charged stripes is discussed in Appendix A. Finally, the results offer strong support for the general picture of stripe phases as stabilized by VHS-induced ordering. A similar approach should be applicable to other systems and, in particular, to nickelates where the coupling to the CDW-breathing mode is known to be stronger.

For the cuprates, we find that the structural distortions are close to the DJT degeneracy, but that the shear and flux phases are more unstable than the CDW. Hence, one would expect significant softening of the breathing modes, but instability in either the shear or flux phase. These expectations are borne out in experiments on the cuprates, with the shear mode coupling to a (local) LTT order. The near degeneracy of the shear and flux phases is consistent with experimental evidence for both modes. It is interesting to note that the molecular analog of the flux phase is a classically chaotic DJT phase. Note that the present results only suggest one possibility: *if* two competing phonon modes are present, then a flux phase will be generated by an electronic DJT effect. However, the operator algebra argument runs both ways: if a flux phase is present, then any coupling to phonons or a CDW will generate the full DJT effect, with competing CDW's.

Recently, DJT phases have been proposed in a number of exotic materials, including cuprates,[15] buckyballs,[12] and manganates.[16] To describe the DJT phase of buckyballs, the concept of Berryonic matter was introduced.[7] In this model, no attempt was made to accurately model buckyball solids. Instead, a lattice of DJT molecules was assumed, basing their properties on the known anomalies associated with triatomic molecules. Since the square molecule, Fig. 2, has the same DJT anomaly as the triangular model when $E^1_{JT}=E^2_{JT}$, and this degeneracy persists on a square lattice (Sec. III C), the present model should be an excellent starting point for studies of Berryonic matter. Moreover, the proximity of the cuprates to the Berryonic limit should stimulate interest in this unusual state of matter.

Finally, the *operator algebra* approach may have an important role in studying competing instabilities. It has already provided a new definition of the DJT effect and shown that related effects can arise in strikingly different physical systems, giving an explicit prescription for determining when two competing order parameters are *miscible*, in the sense that they can coexist by generating a third (hidden) order.

APPENDIX A: PHONONS ON STRIPES

An understanding of the role of phonons in the cuprates is complicated by the possible presence of stripes or other nanoscale phase separation in the hole doped materials. Clearly, any charge modulation will couple to the phonon modes, and the coupling strength will vary from mode to mode, as discussed in Sec. IV. However, it has been postulated[17] that these charged stripes (or domains) are stabilized by a form of CDW. Hence, in this appendix, we briefly review experimental data which seem to provide evidence for an intimate coupling between stripes and particular phonon modes. In such charge inhomogeneous situations, the average structure does not fully characterize the situation, and it is essential to look at local probes of lattice order. Thus, there is considerable evidence for *local LTT* order, even when the average lattice symmetry is orthorhombic LTO—in good agreement with early predictions of nanoscale phase separation.[14,15]

1. Coupling of charged stripes to local LTT order

Long-range LTT order plays an important role in stabilizing a nearly static stripe phase[86] in rare-earth- (RE-) substituted LSCO, where typically RE=Nd or Eu, and LTT anisotropy has been found to help orient stripes.[87,88] While this has been characterized[86] as a pinning effect, it is not necessarily true that LTT order enhances stripe pinning: in Eu-substituted samples, the Cu spins appear to be even more dynamic in the LTT phase.[89] Moreover, such a picture completely fails to explain the common occurrence of *simultaneous* fluctuating stripe order and fluctuating LTT order.

Evidence for dynamic or local LTT order (inequivalent Cu-O bond lengths) has been reviewed several times.[90,29] Recent developments include (1) neutron diffraction pair distribution function (PDF) studies of LSCO (Refs. 91 and 92) find a crossover from local LTO order very near half filling, to a clear mixing of local LTO and LTT order in the doped materials. These doped materials display considerable tilt and bond length disorder, interpretable in terms of stripes. Such a crossover is particularly intriguing in light of the crossover in *stripe orientation* from diagonal at low doping,[93] which could be ''pinned'' by LTO order, to horizontal near optimal doping. This local LTT-LTO-type structural disorder is characteristic of the stripe regime, and the structural disorder greatly reduces[92] near $x=0.25$, close to the point where the stripe phase terminates.[94,54] (2) Bianconi *et al.*[24] report extended x-ray absorption fine structure (EXAFS) evidence for a quantum critical point (QCP)—a local splitting of the Cu-O bond length which can be tuned to zero by adjusting the chemical microstrain. It is found that the highest critical temperatures are associated with this optimal degree of ''microstrain.''[24] (3) Very similar thermal conductivity κ anomalies are found in nickelates and manganites,[95] where κ is suppressed above the charge ordering transition due to collisions between phonons and fluctuating stripes, and in cuprates,[96]*at the LTT transition.* (4) The NQR ''knockout'' effect has been considered to mark the onset of stripe fluctuations;[97] at nearly the same phase boundary x-ray appearance near-edge structure (XANES) (Ref. 98) and PDF (Ref. 92) measurements find the onset of local Cu-O bond length variations suggestive of local LTT-type tilts.

Magnetic field studies provide additional evidence. (5) The Hall effect[99] in strongly Nd-substituted LSCO shows a crossover from one-dimensional ($R_H \to 0$ as $T \to 0$) to two-dimensional behavior at $x=0.12$; for $x<0.12$, the R_H anomaly turns on with stripe order—exactly at the LTT-like phase transition. (6) Further, it is known that an in-plane magnetic field has a strong effect on magnetoresistance, including hysteretic effects which can be interpreted as field-induced rotation of the stripes.[100] Remarkably, an in-plane field also has a strong effect on the LTT-LTO transition temperature,[101] stabilizing the LTT phase at higher T. This can be qualitatively understood if the LTT phase and charge stripes are intimately related: the fluctuating (LTT) stripes are present in the LTO phase, but the strong fluctuations produce an average LTO structural order; the field, by aligning the stripes, reduces transverse fluctuations and reveals the underlying LTT order.

The near coincidence of stripe and structural disorder provides very strong evidence that the two kinds of stripe are associated with two kinds of structural order: that the LTO phase is connected with magnetic stripes, at half filling, and the LTT phase with charged stripes, near optimal doping. The connection between the LTO phase and magnetic stripes may be related to strong magnetoelastic coupling: in the Néel phase, the spin-flop transition is strongly suppressed by LTT order,[89] while in the diagonal stripe phase the cluster spin glass transition can be seen in anelastic relaxation measurements.[102] The Mott insulator $Sr_2CuO_2Cl_2$ (SCOC) is found by x rays to be tetragonal, but below the Néel temperature the infrared absorption peak associated with the Cu-O bending mode phonon is found to split into two components.[103]

In summary, the data suggest the following scenario. The magnetic stripes are associated with a local LTO-type tilt distortion, the charged stripes with an LTT tilting. At half filling, there is a simple long-range LTO order, which may be stabilized by magnetoelastic coupling which aligns the spins with the LTO tilt direction. The LTT tilting, stabilized by coupling to the VHS, is fluctuating unless pinned by ionic disorder off of the CuO_2 planes. When the LTT phase is pinned, the stripes develop long-range charge (and ultimately spin) order. If the stripe pinning is strong enough, the superconducting order can be suppressed, predominantly due to the magnetic order.[104] Near enough to half filling, the LTO tilts prevail, the stripes rotate by 45°, and superconductivity is destroyed.

2. Local breathing order

Tranquada *et al.*[105] found clear indications for the coupling of breathing-mode branches to charge stripe order in the nickelates. Strikingly, there was no indication for a coupling to the stripe periodicity, and the phonons seemed sensitive to local stripe fluctuations. Similar anomalies, particularly involving the half-breathing mode,[19,20] are found in the cuprates and are also considered to be stripe related. In LSCO, stripe correlations have a strong effect on these

oxygen-related phonons near 70 meV.[21,22] In this same energy range (50–70 meV below the Fermi level), photoemission measurements[78–80,18] find a break in the dispersion of the cuprates, which, as discussed above (Sec. V), has been interpreted[18] as due to strong electron-phonon coupling to the breathing-mode phonons.

3. Flux phase on stripes

While early studies suggested that the flux phase *replaces* the antiferromagnetic phase in lightly doped cuprates, the present analysis has antiferromagnetic stripes in the low-doping regime, with the flux phase appearing (if at all) only on the charged stripes. This follows both because instability is enhanced near a VHS and because the correlated hopping scales with x; moreover, in a stripe picture, features near the Fermi level are generally associated with the charged stripes.[54] This conclusion is consistent with the experimental observation[25] that the possible flux related magnetization is stronger in $YBCO_{6+y}$ for $y=0.6$ than for $y=0.35$ (see also Chakravarty, *et al.*[106]). It also provides a natural resolution of the Lee-Wen paradox[107] discussed by Orenstein and Millis.[108] Lee and Wen showed that they could explain the Uemura relation for underdoped cuprates, as long as the flux phase dispersion is independent of doping. The paradox is that many strong-coupling models expect the dispersion to renormalize to zero near the Mott insulator at half filling. In a stripe picture, this renormalization is taken as indicating that the *fraction of material* associated with charged stripes renormalizes to zero at half filling, whereas *the dispersion on a single stripe* is less sensitive to doping.[54]

At very low doping, flux stripes will tend to break up into flux polarons, confined to a single plaquette. These flux polarons bear a close resemblance to the Skyrmions introduced by Gooding.[109] Indeed, his electronic states are just linear combinations of the E_u-symmetry plaquette states of Eq. (9). The difference is that his states are localized around a Sr impurity, while ours are the equilibrium conducting state on the hole-doped stripes. Clearly, at low temperatures there will be a tendency for charged stripes and polarons to be pinned on the Sr, greatly enhancing the similarity. However, the present model more naturally explains stripes at higher-doping levels and the uniform charged phase near x_0. It should be noted that Haskel and co-workers[110,111] find enhanced local structural distortions near Sr impurities, associated with hole localization.

If the flux phase is on the charged stripes, then hole doping will shift the Fermi level away from the conical points, producing not a node but a hole pocket, as in Fig. 6. It is possible that the deviations from d-wave symmetry found in the underdoped regime[112] are associated with this hole pocket. The apparent d-wave gap might then be a *localization* gap at the hole pocket Fermi surface, leading to the localization effects observed in resistivity.[113,114]

APPENDIX B: PHONON MODES IN THE CUPRATES

1. Bond stretching modes in the LSCO three-band model

In Sec. IV, we calculate the mean-field properties of the various CDW's, combining electron-electron and electron-phonon interactions and including strong-coupling corrections and competition with the Mott gap. Here we develop a simple model for estimating the electron-phonon interaction. We introduce a three-band model and apply it to a number of phonon modes which have been proposed to play a role in the cuprates. In the following subsection, we will reduce the model to a one-band version.

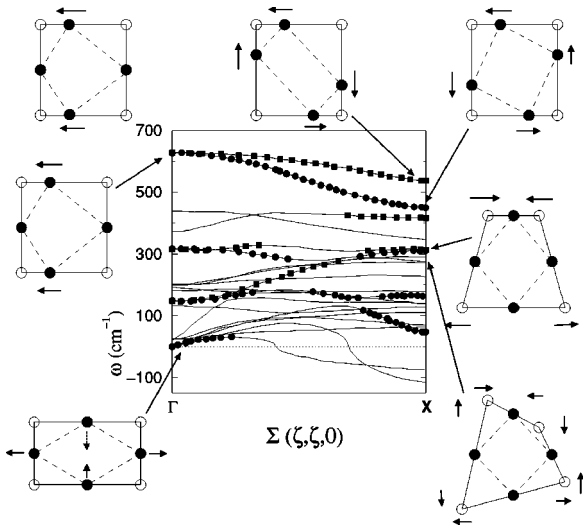

FIG. 9. Phonon modes of the CuO_2 planes, including distortion patterns for several Cu-O bond stretching modes. Clockwise from top left: half-breathing, breathing, quadrupole, dimer I, dimer II, shear, and ferroelectric modes. Solid squares (circles)=Σ_1 (Σ_3) branches predominantly representing the CuO_2 planes.

We concentrate predominantly on CuO_2 plane phonons associated with in-plane vibrations and particularly on Cu-O bond stretching phonons. Mott's original picture of a metal-insulator transition involved a loss of covalency as a lattice is gradually expanded. Hence, near a Mott transition it would be expected that bond length changing phonons might play an important role, modulating a crossover from covalent to ionic behavior.[115] Figure 9 shows the phonon dispersion in La_2CuO_4 along the $(\zeta,\zeta,0)$ (Σ) direction, calculated by Wang *et al.*[116] Shown in bold are the branches which are predominantly associated with in-plane Cu-O vibrations. (Wang *et al.* provide the wave functions only along the high-symmetry axes Γ and X; the remainder of the curves are an interpolation based on symmetry. Note the anticrossing behavior evident on several branches.) The pattern of distortion for a number of modes of interest is also shown, including the breathing,[27] half-breathing[19,115] [at $(\pi,0)$], dimer,[117] quadrupolar,[13] ferroelectric,[115] and shear[33] modes. This by no means exhausts all relevant modes. Among modes which are not modeled are the LTT tilt mode and various c-axis modes.[118] As discussed above, we treat the LTT mode as a secondary modification of the shear mode instability.

In order to estimate how strongly these modes couple to the electrons, we analyze a simple three-band dispersion for the CuO_2 plane, with parameters t_0 (t_1') for Cu-O (O-O) hopping, and Δ_0 (Δ_1) for Cu (O) site energy. The electron-phonon coupling is assumed to arise via modulating these parameters. Thus, a change δu in the Cu-O bond length a produces a change

$$\delta t = -\beta t_0 \delta u/a \tag{B1}$$

in t_0 and a change

$$\delta_0 = \alpha_d \Delta_0 \delta u/a \tag{B2}$$

in Δ_0 (or Δ_1). We estimate $\beta \sim 3.5\alpha_t$ (Refs. 29 and 119) ($\alpha_t = 1$) and α_d from a Madelung contribution as $\alpha_d = qe^2/\epsilon_0 a\Delta_0 \sim 0.55$, for $\Delta_0 \sim 4$ eV, effective charge $q = 2$ (O^{2-} or Cu^{2+}) and dielectric constant $\epsilon_0 \sim 5$. In the following, we will treat the α's as dimensionless parameters of order unity in order to scale the electron-phonon coupling. The net change in Δ on any site is then $(n-m)\delta_0$ where n (m) is the number of near neighbors that move closer to (farther away from) the given site. For a frozen lattice distortion of amplitude $\pm\delta u$, we calculate how the net electronic energy changes. Model parameters include the position of the Fermi level, the value of t_1', and the ratio β/α_d. This last parameter can be thought of as a measure of covalency: increasing Δ tends to localize holes on Cu, making the material more ionic, while increasing t_0 delocalizes holes, increasing covalency. We restrict ourselves here to the following parameters: $t_0 = 1.3$ eV, $\Delta_0 = 4$ eV, $a = 1.9$ Å, Fermi level at VHS (in the absence of phonon distortion) at a doping $x = 0.25$ (to achieve this, a large value of $t_1'/t_0 = -1.8$ is assumed—see the discussion in the following paragraph), and $\alpha_d = \alpha_t = 1$. The model neglects possible coupling to the Cu d_{z^2} orbital (important for the conventional JT distortions of the quadrupole and breathing modes[13]) and anomalies associated with the near instability of O^{2-} (Sec. IV C).[120] The two forms of electron-phonon coupling are similar to those assumed by Yonemitsu *et al.*;[77] while the numerical estimates are not identical, we find similar estimates for the coupling to the breathing mode. Their electron-phonon coupling parameters are, in our notation $\lambda_\alpha = \beta^2 t_0/A_{br} \simeq 0.264$, $\lambda_\beta = \alpha_d^2 \Delta_0^4/t_0 A_{br} \simeq 0.204\alpha_d^2 = 0.051$, for $\alpha_d = 0.5$, and $A_{br} = 60.4$ eV from Table III. Yonemitsu *et al.*[77] estimated $\lambda_\alpha = 0.28$ and had no estimate for λ_β.

In the above list of parameters, one item stands out for particular comment: the large ratio of t_1'/t_0. Actually, there is a well-known problem in the cuprates: that the Fermi surfaces of LSCO and YBCO are different. In the older literature, this is often referred to as a "45° rotation" of the YBCO and Bi2212 Fermi surfaces.[121] In the one-band model, this change can be parametrized by a larger value of the second-neighbor hopping t' for YBCO, by about a factor of 2–3 (typically, $t'/t = -0.16$ to -0.2 in LSCO, -0.5 to -0.6 in YBCO). The same effect arises in the three-band model, where we find that to fit the YBCO Fermi surface, t_1', must be about 3 times as large as found for LSCO. It should be noted that t_1' is an effective parameter, and in reality a number of different physical effects[122,123] contribute to the Fermi surface curvature. Hence, we feel that the large value assumed is justified, in better fitting the Fermi surface found experimentally in YBCO and Bi2212. Had we used the smaller value $t_1'/t_0 \simeq -0.5$ expected for LSCO, our results would change only in that the VHS would fall at a doping ~ 0.16, and the curves in, e.g., Figs. 11 and 8 would be shifted by the ratio 16/25.

For the shear modes and the modes at $S = (\pi, \pi)$, the resulting electronic Hamiltonian can be written in the form

$$H = \begin{pmatrix} \Delta+\delta_1 & -t_1 e_x & -t_2 e_y & 0 & t_3 e_x^* & t_4 e_y^* \\ -t_1^* e_x^* & \delta_2 & -2t_1' c_-' & t_5 e_x & 0 & -2t_1' c_+' \\ -t_2^* e_y^* & -2t_1' c_-' & \delta_3 & t_6 e_y & -2t_1' c_+' & 0 \\ 0 & t_5^* e_x^* & t_6^* e_y^* & \Delta-\delta_1 & -t_7 e_x & -t_8 e_y \\ t_3^* e_x & 0 & -2t_1' c_+' & -t_7^* e_x^* & -\delta_4 & -2t_1' c_-' \\ t_4^* e_y & -2t_1' c_+' & 0 & -t_8^* e_y^* & -2t_1' c_-' & -\delta_5 \end{pmatrix}, \tag{B3}$$

while for the half-breathing mode at $X = (\pi, 0)$ and the ferroelectric mode,

$$H = \begin{pmatrix} \Delta+\delta_1 & -t_1 e_x & -2it_0 s_y' & 0 & t_3 e_x^* & 0 \\ -t_1 e_x^* & 0 & -2it_1' s_y' e_x & t_5 e_x & 0 & 2it_1' s_y' e_x^* \\ 2it_0 s_y' & 2it_1' s_y' e_x^* & \overline{\delta_3} & 0 & 2it_1' s_y' e_x & 0 \\ 0 & t_5 e_x^* & 0 & \Delta-\delta_1 & -t_7 e_x & -2it_0 s_y' \\ t_3 e_x & 0 & -2it_1' s_y' e_x^* & -t_7 e_x^* & 0 & -2it_1' s_y' e_x \\ 0 & -2it_1' s_y' e_x & 0 & 2it_0 s_y' & 2it_1' s_y' e_x^* & -\overline{\delta_3} \end{pmatrix}. \tag{B4}$$

TABLE I. Phonon coupling parameters.

Mode	n_1	n_2	n_3	m_1	m_2	m_3	m_4
(1) Breathing	4	0	0	1	1	1	1
(2) Half-breathing	2	0	2′	1	–	1	–
(3) Quadrupolar	0	0	0	1	-1	1	-1
(4) Dimer I	0	-2	0	1	0	-1	0
(5) Dimer II	0	-2	2	1	-1	-1	1
(6) Dimer III	0	-2	2	1	1	-1	-1
(7) Shear	0	-2	2	1	-1	1	-1
(8) Ferroelectric	0	0	0	1	–	-1	–

Here $e_i=\exp(ik_ia/2)$, $i=x,y$, $c'_\pm=\cos(k_x\pm k_y)a/2$, and $s'_y=\sin k_ya/2$. For the modes at S (the shear mode), $\delta_{i+2}=\delta_i$ $(-\delta_i)$, $i=2,3$. Writing $\delta_i=n_i\delta_0$ and $t_i=t_0+m_i\delta t_0$, then for oxygen vibrations (the breathing, half-breathing, ferroelectric, and quadrupole modes) $m_{i+4}=+m_i$, while for modes involving copper motions (the shear and dimers), $m_{i+4}=-m_i$, $i=1,4$. For completeness, we include an extra parameter $\overline{\delta_3}$ in Eq. (B4) which is allowed by symmetry, due to second-neighbor relative motion; however, to make a uniform comparison with other modes, the value of $\overline{\delta_3}$ will be set to zero. The remaining elements are listed in Table I.

The above calculations refer to static (frozen) phonon modes, and hence do not give direct information on DJT modes. In a Hartree-Fock calculation, dynamic modes can be modeled by imaginary order parameters, and in Sec. IV, it is shown that the mean-field decomposition of nearest-neighbor Coulomb repulsion produces a direct coupling to the OAF (flux-phase) mode. In this spirit a similar mean-field phonon flux phase can be constructed from the above by (a) replacing δt_0 by $i\,\delta t_0$ and (b) making a similar replacement for the δ_i, which involves moving the term to the off-diagonal $(H_{i,i+3})$ position.

The lattice distortions are found by minimizing the sum of the Hamiltonian, Eq. (B4), and a phonon term, Eq. (12), which may be rewritten as $H_{ph}=A(\delta u/a)^2$, where $A=\eta M\omega^2a^2/2$, and A and ω are listed in Table III. Strictly speaking, the phonon frequencies should be bare values, neglecting electron-phonon coupling, but for present purposes we use calculated[116] or experimental[30] values for the undoped insulator La_2CuO_4. [For the shear mode, $A=(C_{11}-C_{12})a^2c$, where $(C_{11}-C_{12})/2=99$ GPa (Ref. 32) and c is the c-axis lattice constant.] The parameter η is 1 if the distortion is along the X or Y axis only, 2 if it is along both, and M is the mass of the moving ion, oxygen or copper (or the appropriate average for the ferroelectric mode). These equations must in general be solved numerically, but some insight can be gotten for the special case $n_2=n_3=t'_1=0$, for which the four nonzero eigenvalues are given by

$$E_{i\pm}=\frac{\Delta_0\pm\sqrt{\Delta_0^2+4W_i^2}}{2}, \tag{B5}$$

with $i=\pm1$, $W_\pm^2=W_1^2\pm\sqrt{X_1^2+|X_2|^2}$, $W_1^2=4[t_0^2+(1-\gamma/2)\delta t_0^2]$ (except for the half-breathing and ferroelectric (FE) modes, for which $W_1^2=2(t_0^2[1+2s_y'^2]+\delta t_0^2)$) and the

TABLE II. Energy parameters.

Mode	γ	X_1	X_2
(1) Breathing	0	$2X_{10}$	X_-
(2) Half-breathing	0	X_{10}	$2(t_0^2-\delta t_0^2)c_x$
(3) Quadrupolar	0	0	X_-
(4) Dimer I	1	0	$X_++4it_0\delta t_0s_x$
(5) Dimer II	0	0	$X_++4it_0\delta t_0(s_x-s_y)$
(6) Dimer III	0	0	$X_++4it_0\delta t_0(s_x+s_y)$
(7) Shear	0	0	$2(t_+^2c_x+t_-^2c_y)$
(8) Ferroelectric	0	0	$2(t_0^2-\delta t_0^2)c_x$
(9) Flux dimer I	1	0	$X_-+4it_0\delta t_0c_x$
(10) Flux dimer II	0	0	$X_-+4it_0\delta t_0(c_x-c_y)$
(11) Flux dimer III	0	0	$X_-+4it_0\delta t_0(c_x+c_y)$
(12) Flux shear	0	0	$X_--4t_0\delta t_0(s_x-s_y)$

X's and γ's are listed in Table II, with $s_i=\sin(k_ia)$ [and recall $c_i=\cos(k_ia)$], $X_\pm=2(t_0^2\pm\delta t_0^2)(c_x+c_y)\mp2\gamma\delta t_0^2c_y$, and $X_{10}=2E\delta_1+4t_0\delta t_0$ (note that the solution is only implicit if $\delta_1\neq0$). The generic form of X_2 is $X_2=t_1t_5e_x^2+t_3^*t_7^*e_x^{*2}+t_2t_6e_y^2+t_4^*t_8^*e_y^{*2}$. Note that E_{i+} is the antibonding band which is approximately half filled.

Figure 10 shows the calculated electronic energy shifts up to large distortions $\delta u/a=0.1$ (local distortions of up to about 5% are reported in EXAFS measurements[24]). A number of interesting features can be noted. (1) All the distortions lead to highly nonlinear shifts of the electronic energy. (2) While the breathing mode has the strongest coupling (as originally predicted by Weber[27]), the half-breathing mode also has a large coupling, since δ_1 produces a large splitting at the VHS (Fig. 12, below). (3) The energy shifts correspond to significant phonon softening, but when the quadratic phonon energy is included, it is found that only the breathing and (marginally) half-breathing mode become unstable—the additional softening due to electron-electron coupling is discussed in Sec. IV A. Instabilities of the dimer

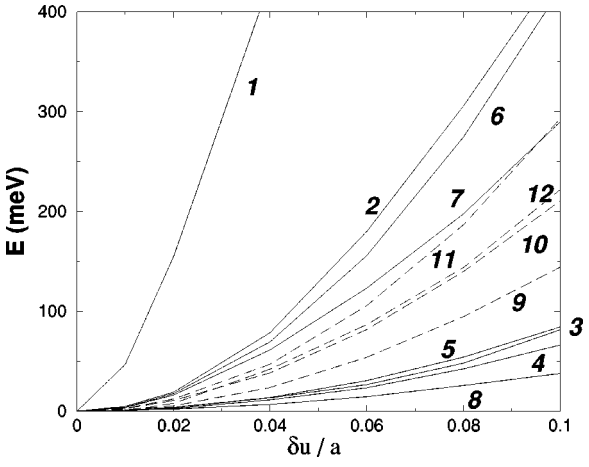

FIG. 10. Energy of various phonon modes of CuO_2 planes, assuming $\alpha_d=1$ and $\beta=3.5$, for static (solid lines) or flux phases (dashed lines). The phonon modes are numbered according to Table II.

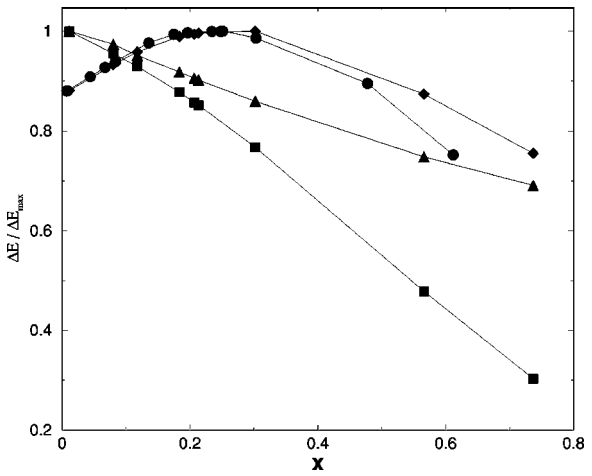

FIG. 11. Doping dependance of the frozen phonon energy lowerings, associated with the breathing mode (circles), half-breathing $(\pi/a,0)$ mode (squares), shear mode (diamonds), and dimer III mode (triangles), all normalized to their maximum amplitude. The half-breathing and shear modes have strongest coupling near the VHS. $\delta u/a=0.04$ for the breathing mode, 0.08 for the others.

modes were found earlier,[117] but only in strong-nesting conditions—half filling with $t_1'=0$. (4) The asymmetric (c_x-c_y) phonon-flux (dimer II) mode has a smaller energy lowering than the symmetric dimer III mode.

The doping dependence of the energy lowering is shown in Fig. 11. The results are in good agreement with experiments[19] on both LSCO and YBCO and with local density approximation (LDA) calculations[124] which find that the half-breathing mode softens more than the (π,π) breathing mode. This result is surprising since the breathing mode has stronger coupling. However, this mode has an unusual frustration effect: it opens a complete gap at the Fermi level, Fig. 12, so the Fermi level can only fall in the gap if the band is filled, $x=0$. To accomodate additional holes, the Fermi level

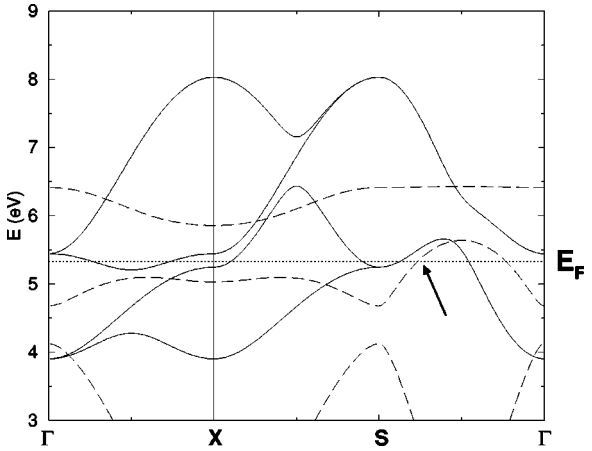

FIG. 12. Three-band dispersion of the CuO_2 planes, in the presence of a frozen breathing mode (dashed lines) or half-breathing $(\pi/a,0)$ mode (solid lines) modulation, assuming $\beta/\alpha_d=3.5$, and $\delta u/a=0.02$ (breathing) or 0.04 (half-breathing). The arrow indicates the breathing mode hole pocket near $(\pi/2a,\pi/2a)$. Brillouin zone special points are $\Gamma=(0,0)$, $X=(\pi/a,0)$, and $S=(\pi/a,\pi/a)$.

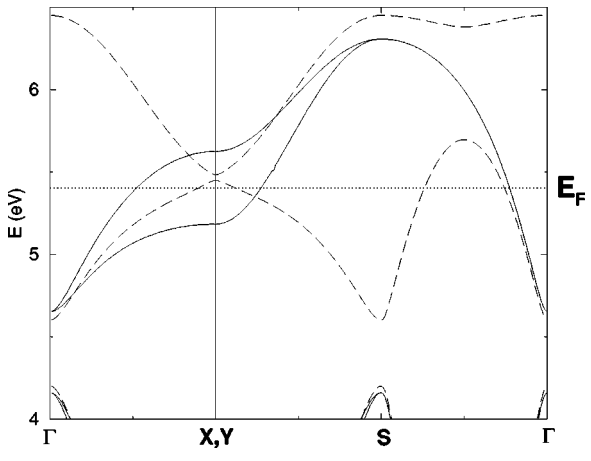

FIG. 13. Three-band dispersion of the CuO_2 planes, in the presence of a frozen dimer II mode (long-dashed lines) or shear mode (solid lines) modulation, assuming $\beta/\alpha_d=3.5$, and $\delta u/a=0.04$.

must shift *below* the gap, reducing the electronic energy lowering. Hence optimal doping for this mode is at half filling, and *while there is a large electronic softening of the breathing mode at the VHS, there is an even larger softening near half filling, so a doping dependence would show a hardening of the mode*. Indeed, such a hardening is observed in the nickelates.[105] This result persists in the presence of strong correlation effects, Sec. IV. For the half-breathing mode correlation effects should enhance the already large softening of the mode with doping, in good agreement with experiment.

Figures 12–14 compare the dispersions of several of the modes, near the upper (Cu-like) band of the three-band model. For all cases, the magnitude of electronic energy lowering can be directly correlated with the size of the gap at the VHS (X point). Note that the gap is largest for the breathing mode, but the Fermi level lies below the gap if $x\neq 0$. For the modes at Γ, there is no unit cell doubling, but the dispersion is different along X and Y, leading to an effective splitting of the VHS's, Figs. 13 and 14.

For the half-breathing mode we find that the softening is via the on-site Cu energy Δ. Making Δ inequivalent on al-

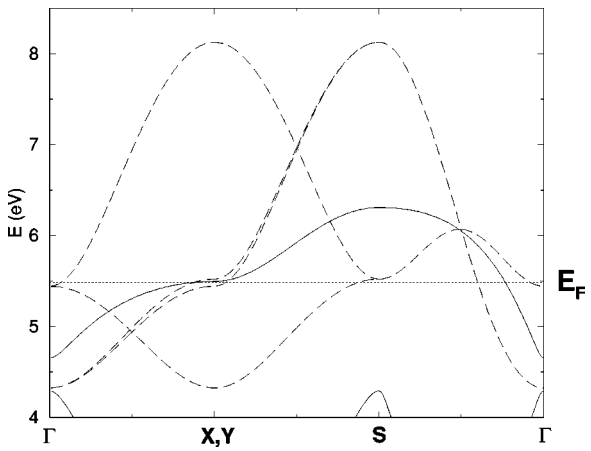

FIG. 14. Three-band dispersion of the CuO_2 planes, in the presence of a frozen ferroelectric (solid lines) or quadrupole mode (dashed lines) modulation, assuming $\beta/\alpha_d=3.5$, and $\delta u/a=0.08$.

ternative rows of Cu atoms along the X axis (parallel to the oxygen distortion) leads to a large splitting of the VHS's. Figure 12 shows that the gap is smaller than for the full breathing mode, but is clearly centered at the VHS.

2. Bond stretching modes in the LSCO one-band model

To combine the phonons with the electron-electron coupling of Sec. IV A, it is convenient to first reduce the above results to a one-band model. The parameters of the one-band model can readily be related to those of the three-band model by expanding the approximate eigenvalues of Eq. (B5) as $E_{i+}=\Delta_0+W_i^2/\Delta_0$. In this way, it is found that the effective Cu-Cu hopping parameter is $t=t_0^2/\Delta_0$ (with the parameters assumed above, this would give $t=0.42$ eV, somewhat larger than the value 0.326 eV estimated from photoemission), with phonon distortion parameters $\delta t/t=2\,\delta t_0/t_0$ and $\overline{\delta_1}=\delta_0+\delta t$. Linearizing the results in δt_0, it is readily seen that the flux dimer II mode has the symmetry of the conventional flux phase, and it is found that the quadrupole and ferroelectric modes do not couple at the one-band level, while the breathing mode couples only via $\overline{\delta_1}$. The electronic dispersion can be solved:

$$E=-4t'c_xc_y\pm\sqrt{(m_1\overline{\delta_1})^2+|X_1+X_2|^2}, \tag{B6}$$

with m_1 and X_2 listed in Table III, and $X_1=-2t(c_x+c_y)$. The result for the half-breathing mode is distinct:

$$E=-2tc_y\pm\sqrt{(2\overline{\delta_1}-2\overline{\delta t c_y})^2+4(t+2t'c_y)^2c_x^2}. \tag{B7}$$

The resulting dispersions are in excellent agreement with the corresponding antibonding band dispersions of the three-band model.

For the half-breathing mode the term in $\overline{\delta t}$ follows from the $\overline{\delta_3}$ term in Eq. (B4): for a phonon distortion along X, the hopping along Y is modified along alternate rows, at $t\sim t_0^2/(\Delta_0\pm\overline{\delta_3})$. Such a term has been previously considered by Shen *et al.*[18] In the present comparisons of different modes, the role of such a term has been neglected (by setting $\overline{\delta_3}=0$).

Equation (B6) bears a strong formal resemblance to Eq. (29). In fact, the one-band model linear electron-phonon coupling has exactly the same form as the V electron-electron term in Eq. (28) for all three CDW modes. Thus, the free energy F_1, Eq. (32), is a function only of the *sums* of the electron-electron and electron-phonon gaps, leading to a simplification of the gap equations. For example, for the CDW, $F_1=F_1(R_{z0}+4\,\delta_1)$, so

$$\left\langle\frac{\partial F_1}{\partial\delta_1}\right\rangle=4\left\langle\frac{\partial F_1}{\partial R_{z0}}\right\rangle. \tag{B8}$$

Since the averages are just those evaluated in the gap equations, they can be replaced by the derivatives of the quadratic terms, yielding

$$\eta_z=\frac{4\,\overline{\delta_1}}{R_{z0}}=\frac{16\alpha_d^2\Delta_0^2}{A(8V-U)}. \tag{B9}$$

For the shear and flux modes, the equivalent result is

$$\eta_i=\frac{2\,\delta t}{R_{i0}}=\frac{4\beta^2t^2}{A_iV}, \tag{B10}$$

with $\beta=3.5\alpha_t$. These are the analogs to Eq. (13). They are weak-coupling results and should be modified when the gaps become comparable to the phonon frequencies. In the evaluation of these equations, in Eqs. (34)–(36), we assume the parameter values of Table III and give the α's their nominal values, $\alpha_d=0.5$, $\alpha_t=1$.

TABLE III. One-band model parameters.

Mode	m_1	X_2	ω (meV)	A (eV)
(1) Breathing	4	0	66	60.4
(2) Half-breathing	2	–	83	47.8
(3) Quadrupolar	0	0	56	43.5
(4) Dimer I	0	$-2i\,\delta t s_x$	38	39.7
(5) Dimer II	0	$-2i\,\delta t(s_x+s_y)$	38	79.5
(6) Dimer III	0	$-2i\,\delta t(s_x-s_y)$	38	79.5
(7) Shear	0	$-2\,\delta t(c_x-c_y)$	–	59
(8) Ferroelectric	0	0	77	32.8
(9) Flux dimer I	0	$-2i\,\delta t c_x$	38	39.7
(10) Flux dimer II	0	$-2i\,\delta t(c_x-c_y)$	38	79.5
(11) Flux dimer III	0	$-2i\,\delta t(c_x+c_y)$	38	79.5
(12) Flux shear	0	$+2i\,\delta t(s_x-s_y)$	–	59

[1] I. Affleck and J.B. Marston, Phys. Rev. B **37**, 3774 (1988).

[2] R.B. Laughlin, J. Phys. Chem. Solids **56**, 1627 (1995); X.-G. Wen and P.A. Lee, Phys. Rev. Lett. **76**, 503 (1996).

[3] E. Cappelluti and R. Zeyher, Phys. Rev. B **59**, 6475 (1999).

[4] B.I. Halperin and T.M. Rice, in *Solid State Physics*, edited by F. Seitz, D. Turnbull, and H. Ehrenreich (Academic, New York, 1968), Vol. 21, p. 115.

[5] H.J. Schulz, Phys. Rev. B **39**, 2940 (1989).

[6] D.A. Ivanov, P.A. Lee, and X.-G. Wen, Phys. Rev. Lett. **84**, 3958 (2000); S. Chakravarty, R.B. Laughlin, D.K. Morr, and C. Nayak, Phys. Rev. B **63**, 094503 (2001); see also D.J. Scalapino and S.R. White, Found. Phys. **31**, 27 (2001).

[7] N. Manini, E. Tosatti, and S. Doniach, Phys. Rev. B **51**, 3731 (1995); G. Santoro, M. Airoldi, N. Manini, E. Tosatti, and A. Parola, Phys. Rev. Lett. **74**, 4039 (1995); D. Shelton and A.M. Tsvelik (unpublished).

[8] G. Herzberg and H.C. Longuet-Higgins, Discuss. Faraday Soc. **35**, 77 (1963).

[9] H. von Busch, Vas Dev, H.-A. Eckel, S. Kasahara, J. Wang, W. Demtröder, P. Sebald, and W. Meyer, Phys. Rev. Lett. **81**, 4584 (1998).

[10] R. Englman and B. Halperin, Phys. Rev. B **2**, 75 (1970); B. Hal-

perin and R. Englman, *ibid.* **3**, 1698 (1971).
[11] I.B. Bersuker and V.Z. Polinger, *Vibronic Interactions in Molecules and Crystals* (Springer, Berlin, 1989).
[12] C.M. Varma, J. Zaanen, and K. Raghavachari, Science **254**, 989 (1991); M. Lannoo, G.A. Baraff, M. Schlüter, and D. Tomanek, Phys. Rev. B **44**, 12 106 (1991); M. Schlüter, M. Lannoo, M. Needels, G.A. Baraff, and D. Tománek, Phys. Rev. Lett. **68**, 526 (1992); Mater. Sci. Eng., B **19**, 129 (1993); V.P. Antropov, O. Gunnarsson, and A.I. Liechtenstein, Phys. Rev. B **48**, 7651 (1993); A. Auerbach, Phys. Rev. Lett. **72**, 2931 (1994).
[13] K.A. Müller, J. Supercond. **12**, 3 (1999).
[14] R.S. Markiewicz, Physica C **200**, 65 (1992).
[15] R.S. Markiewicz, Physica C **210**, 235,264 (1993).
[16] A.J. Millis, P.B. Littlewood, and B.I. Shraiman, Phys. Rev. Lett. **74**, 5144 (1995); A.J. Millis, B.I. Shraiman, and R. Mueller, *ibid.* **77**, 175 (1996); A.J. Millis, Phys. Rev. B **53**, 8434 (1996).
[17] R.S. Markiewicz, J. Phys.: Condens. Matter **2**, 665 (1990).
[18] A. Lanzara, P.V. Bogdanov, X.J. Zhou, S.A. Kellar, D.L. Feng, E.D. Lu, T. Yoshida, H. Eisaki, A. Fujimori, K. Kishio, J.-I. Shimoyama, T. Noda, S. Uchida, Z. Hussain, and Z.-X. Shen, Nature (London) **412**, 510 (2001); Z.-X. Shen, A. Lanzara, S. Ishihara, and N. Nagaosa, cond-mat/0108381 (unpublished).
[19] R.J. McQueeney, Y. Petrov, T. Egami, M. Yethiraj, G. Shirane, and Y. Endoh, Phys. Rev. Lett. **82**, 628 (1999).
[20] Y. Petrov, T. Egami, R.J. McQueeney, M. Yethiraj, H.A. Mook, and F. Dogan, cond-mat/0003414 (unpublished).
[21] R.J. McQueeney, J.L. Sarrao, P.G. Pagliuso, P.W. Stephens, and R. Osborn, Phys. Rev. Lett. **87**, 077001 (2001).
[22] R.J. McQueeney, J.L. Sarrao, J.S. Gardner, M.F. Hundley, and R. Osborn, Phys. Rev. B **60**, 80 (1999).
[23] L. Pintschovius and M. Braden, Phys. Rev. B **60**, 15 039 (1999).
[24] A. Bianconi, G. Bianconi, S. Caprara, D. Di Castro, H. Oyanagi, and N.L. Saini, J. Phys.: Condens. Matter **12**, 10 655 (2000).
[25] H.A. Mook, Pengcheng Dai, and F. Dogan, Phys. Rev. B **64**, 012502 (2001); H. Mook (unpublished); B. Keimer (unpublished).
[26] R.S. Markiewicz, Bull. Am. Phys. Soc. **43**, 320 (1998); R.S. Markiewicz, C. Kusko, and M.T. Vaughn, *ibid.* **44**, 460 (1999).
[27] W. Weber, Phys. Rev. Lett. **58**, 1371 (1987).
[28] M. Grilli and C. Castellani, Phys. Rev. B **50**, 16 880 (1994); F. Becca, M. Tarquini, M. Grilli, and C. di Castro, *ibid.* **54**, 12 443 (1996).
[29] R.S. Markiewicz, J. Phys. Chem. Solids **58**, 1179 (1997).
[30] L. Pintschovius and W. Reichardt, in *Physical Properties of High Temperatures IV*, edited by D.M. Ginsberg (World Scientific, Singapore, 1994), p. 295.
[31] M. Braden, W. Paulus, A. Cousson, P. Vigoureux, G. Heger, A. Goukassov, P. Bourges, and D. Petitgrand, Europhys. Lett. **25**, 625 (1994); M. Braden, P. Adelmann, W. Paulus, P. Vigoureux, G. André, P. Schweiss, A. Cousson, A. Goukassov, S.N. Barilo, D.I. Zhigounov, and G. Heger, Physica C **235-240**, 793 (1994).
[32] M. Nohara, T. Suzuki, Y. Maeno, T. Fujita, I. Tanaka, and H. Kojima, Phys. Rev. Lett. **70**, 3447 (1993); S. Sakita, T. Suzuki, F. Nakamura, M. Nohara, Y. Maeno, and T. Fujita, Physica B **219-220**, 216 (1996).
[33] R.S. Markiewicz, Physica C **255**, 211 (1995).
[34] A.P. Giddy, M.T. Dove, G.S. Pawley, and V. Heine, Acta Crystallogr., Sect. A: Found. Crystallogr. **49**, 697 (1993); M.T. Dove, V. Heine, and K.D. Hammonds, Miner. Mag. **59**, 629 (1995).
[35] C.J. Halboth and W. Metzner, Phys. Rev. Lett. **85**, 5162 (2000).
[36] B. Valenzuela and M.A.H. Vozmediano, Phys. Rev. B **63**, 153103 (2001).
[37] P. Schweiss, W. Reichardt, M. Braden, G. Collin, G. Heger, H. Claus, and A. Erb, Phys. Rev. B **49**, 1387 (1994).
[38] J. Röhler, Physica B **284-88**, 1041 (2000).
[39] O.K. Andersen, A.I. Liechtenstein, O. Rodriguez, I.I. Mazin, O. Jepsen, V.P. Antropov, O. Gunnarson, and S. Gopolan, Physica C **185-189**, 147 (1991).
[40] V. Pasler, P. Schweiss, C. Meingast, B. Obst, H. Wühl, A.I. Rykov, and S. Tajima, Phys. Rev. Lett. **81**, 1094 (1998).
[41] E. Kaldis, J. Röhler, E. Liarokapis N. Poulakis, K. Conder, and P.W. Loeffen, Phys. Rev. Lett. **79**, 4894 (1997).
[42] M.C. Schnabel, C.-H. Park, A. Matsuura, Z.-X. Shen, D.A. Bonn, R. Liang, and W.N. Hardy, Phys. Rev. B **57**, 6090 (1998); **57**, 6107 (1998); also D.H. Lu, D.L. Feng, N.P. Armitage, K.M. Shen, A. Damascelli, C. Kim, F. Ronning, Z.-X. Shen, D.A. Bonn, R. Liang, W.N. Hardy, A.I. Rykov, and S. Tajima, Phys. Rev. Lett. **86**, 4370 (2001).
[43] H.A. Mook and F. Doğan, Nature (London) **401**, 145 (1999); Physica C **364-365**, 553 (2001).
[44] O. Chmaissem, J.D. Jorgensen, S. Short, A. Knizhnik, Y. Eckstein, and H. Shaked, Nature (London) **397**, 45 (1999).
[45] D.J. Singh and W.E. Pickett, J. Supercond. **8**, 583 (1995).
[46] P. Aebi, J. Osterwalder, P. Schwaller, L. Schlapbach, M. Shimoda, T. Mochiku, and K. Kadowaki, Phys. Rev. Lett. **72**, 2757 (1994).
[47] A.A. Kordyuk, S.V. Borisenko, M.S. Golden, S. Legner, K.A. Nenkov, M. Knupfer, J. Fink, H. Berger, and L. Forro, cond-mat/0104294 (unpublished).
[48] M. Braden, W. Reichardt, E. Elkaim, J.P. Lauriat, S. Shiryaev, and S.N. Barilo, Phys. Rev. B **62**, 6708 (2000).
[49] A.I. Solomon and J.L. Birman, J. Math. Phys. **28**, 1526 (1987).
[50] R.S. Markiewicz and M.T. Vaughn, Phys. Rev. B **57**, 14 052 (1998); J. Phys. Chem. Solids **59**, 1737 (1998); in *Particles, Strings, and Cosmology (PASCOS98)*, edited by P. Nath (World Scientific, Singapore, 1999), p. 771.
[51] S.-C. Zhang, Science **275**, 1089 (1997).
[52] C. Henley, Phys. Rev. Lett. **80**, 3590 (1998).
[53] J. Zaanen and P.B. Littlewood, Phys. Rev. B **50**, 7222 (1994).
[54] R.S. Markiewicz, Phys. Rev. B **62**, 1252 (2000).
[55] R.S. Markiewicz and C. Kusko, Phys. Rev. B **65**, 064520 (2002).
[56] D.V. Fil, O.I. Tokar, A.L. Shelankov, and W. Weber, Phys. Rev. B **45**, 5633 (1992); M.D. Kaplan and G.O. Zimmerman, J. Phys. Chem. Solids **59**, 1831 (1998).
[57] G.I. Bersuker and J.B. Goodenough, Physica C **274**, 267 (1997).
[58] A.S. Moskvin, E.N. Kondrashov, and V.I. Cherepanov, Phys. Solid State **43**, 823 (2001).
[59] M.D. Kaplan and B.G. Vekhter, *Cooperative Phenomena in Jahn-Teller Crystals* (Plenum, New York, 1995).
[60] R.S. Markiewicz, Phys. Rev. E **64**, 026216 (2001); in *Vibronic Interactions: Jahn-Teller Effect in Crystals and Molecules*, edited by M.D. Kaplan and G.O. Zimmerman (Kluwer, Dordrecht, 2001), p. 273.
[61] C.A. Mead, Rev. Mod. Phys. **64**, 51 (1992).
[62] M.V. Berry, Proc. R. Soc. London, Ser. A **392**, 45 (1984).
[63] M. Bacci, Phys. Rev. B **17**, 4495 (1978).
[64] S. Flach, N.M. Plakida, and V.L. Aksenov, Int. J. Mod. Phys. B **4**, 1955 (1990); W.E. Pickett, R.E. Cohen, and H. Krakauer, Phys. Rev. Lett. **67**, 228 (1991); A. Bussmann-Holder, A. Migliori, Z.

Fisk, J.L. Sarrao, R.G. Leisure, and S.-W. Cheong, *ibid.* **67**, 512 (1991).
[65] R.L. Melcher, in *Physical Acoustics*, edited by W.P. Mason and R.N. Thurston (Academic, New York, 1976), Vol. 12, p. 1.
[66] G.C. Psaltakis and E.W. Fenton, J. Phys. C **16**, 3913 (1983): M. Murakami and H. Fukuyama, J. Phys. Soc. Jpn. **67**, 2784 (1998).
[67] M. Murakami, J. Phys. Soc. Jpn. **69**, 1113 (2000).
[68] Note that the symmetries of the elements may lead to a larger subgroup. Thus when the elements are AFM and DSC, the associated group is SO(5).
[69] F. Barriquand and G.A. Sawatzky, Phys. Rev. B **50**, 16 649 (1994).
[70] C. Nayak, Phys. Rev. B **62**, 4880 (2000).
[71] T.D. Stanescu and P. Phillips, Phys. Rev. B **64**, 220509 (2001).
[72] T. Hsu, J.B. Marston, and I. Affleck, Phys. Rev. B **43**, 2866 (1991).
[73] H. Bilz, G. Benedek, and A. Bussmann-Holder, Phys. Rev. B **35**, 4840 (1987).
[74] A. Bussmann-Holder, A. Simon, and H. Büttner, Phys. Rev. B **39**, 207 (1989).
[75] J.E. Hirsch and F. Marsiglio, Phys. Rev. B **39**, 11 515 (1989); **45**, 4807 (1992).
[76] R.S. Markiewicz, C. Kusko, and V. Kidambi, Phys. Rev. B **60**, 627 (1999).
[77] K. Yonemitsu, A.R. Bishop, and J. Lorenzana, Phys. Rev. B **47**, 12 059 (1993).
[78] P.V. Bogdanov, A. Lanzara, S.A. Kellar, X.J. Zhou, E.D. Lu, W. Zheng, G. Gu, K. Kishio, J.-I. Shimoyama, Z. Hussain, and Z.X. Shen, Phys. Rev. Lett. **85**, 2581 (2000).
[79] A. Kaminski, M. Randeria, J.C. Campuzano, M.R. Norman, H. Fretwell, J. Mesot, T. Sato, T. Takahashi, and K. Kadowaki, Phys. Rev. Lett. **86**, 1070 (2001).
[80] T. Valla, Bull. Am. Phys. Soc. **46**, 289 (2001); Z. Yusov, B.O. Wells, T. Valla, A.V. Fedorov, P.D. Johnson, Q. Li, G.D. Gu, N. Koshizuka, C. Kendziora, S. Jian, and D.G. Hinks, *ibid.* **46**, 1039 (2001) [figure in N. Smith, Phys. Today **54** (1), 33 (2001)].
[81] R.S. Markiewicz, Physica C **168**, 195 (1990).
[82] C. Kusko, Z. Zhai, N. Hakim, R.S. Markiewicz, S. Sridhar, D. Colson, Viallet-Guillet, A. Forget, Yu.A. Nefyodov, M.R. Trunin, N.N. Kolesnikov, A. Maignan, A. Daignere, and A. Erb, Phys. Rev. B **65**, 132501 (2002).
[83] A.V. Chubukov and K.A. Musaelian, J. Phys.: Condens. Matter **7**, 133 (1995).
[84] C. Kusko, R.S. Markiewicz, M. Lindroos, and A. Bansil, cond-mat/0201117 (unpublished).
[85] N.P. Armitage, D.H. Lu, C. Kim, A. Damascelli, K.M. Shen, F. Ronning, D.L. Feng, H. Eisaki, Z.-X. Shen, P.K. Mang, N. Kaneko, M. Greven, Y. Onose, Y. Taguchi, and Y. Tokura, cond-mat/0201119, Phys. Rev. Lett. (to be published).
[86] J.M. Tranquada, B.J. Sternlieb, J.D. Axe, Y. Nakamura, and S. Uchida, Nature (London) **375**, 561 (1995); J.M. Tranquada, J.D. Axe, N. Ichikawa, A.R. Moodenbaugh, Y. Nakamura, and S. Uchida, Phys. Rev. Lett. **78**, 338 (1997).
[87] B. Normand and A.P. Kampf, Phys. Rev. B **64**, 024521 (2001).
[88] A.P. Kampf, D.J. Scalapino, and S.R. White, Phys. Rev. B **64**, 052509 (2001).
[89] V. Kataev, A. Validov, M. Hücker, H. Berg, and B. Büchner, J. Phys.: Condens. Matter **11**, 6571 (1999).
[90] T. Egami and S.J.L. Billinge, in *Phyical Properties of High T Superconductors V*, edited by D.M. Ginsberg (World Scientific, Singapore, 1996).
[91] E.S. Božin, S.J.L. Billinge, G.H. Kwei, and H. Takagi, Phys. Rev. B **59**, 4445 (1999).
[92] E.S. Božin, G.H. Kwei, H. Takagi, and S.J.L. Billinge, Phys. Rev. Lett. **84**, 5856 (2000); M. Gutmann, E.S. Božin, and S.J.L. Billinge, cond-mat/0009141 (unpublished).
[93] S. Wakimoto, G. Shirane, Y. Endoh, K. Hirota, S. Ueki, K. Yamada, R.J. Birgeneau, M.A. Kastner, Y.S. Lee, P.M. Gehring, and S.H. Lee, Phys. Rev. B **60**, 769 (1999); S. Wakimoto, R.J. Birgeneau, M.A. Kastner, Y.S. Lee, R. Erwin, P.M. Gehring, S.H. Lee, M. Fujita, K. Yamada, Y. Endoh, K. Hirota, and G. Shirane, *ibid.* **61**, 3699 (2000).
[94] J.L. Tallon, *Advances in Superconductivity XII* (Springer, Tokyo, 2000), p. 185; J.L. Tallon, J.W. Loram, and G.V.M. Williams, Physica C **338**, 9 (2000); J.L. Tallon, J.W. Loram, G.V.M. Williams, J.R. Cooper, I.R. Fisher, J.D. Johnson, M.P. Staines, and C. Bernhard, Phys. Status Solidi B **215**, 531 (1999).
[95] C. Hess, B. Büchner, M. Hücker, R. Gross, and S.-W. Cheong, Phys. Rev. B **59**, 10 397 (1999).
[96] O. Baberski, A. Lang, O. Maldonado, M. Hücker, B. Büchner, and A. Freimuth, Europhys. Lett. **44**, 335 (1998).
[97] P.M. Singer, A.W. Hunt, A.F. Cederström, and T. Imai, Phys. Rev. Lett. **82**, 4300 (1999).
[98] N.L. Saini, H. Oyanagi, and A. Bianconi, J. Synchrotron. Radiat. (to be published).
[99] T. Noda, H. Eisaki, and S. Uchida, Science **286**, 265 (1999).
[100] Y. Ando, A.N. Lavrov, and K. Segawa, Phys. Rev. Lett. **83**, 2813 (1999).
[101] Z.A. Xu, N.P. Ong, T. Noda, H. Eisaki, and S. Uchida, Europhys. Lett. **50**, 796 (2000).
[102] A. Campana, R. Cantelli, F. Cordero, M. Corti, and A. Rigamonti, Eur. Phys. J. B **18**, 49 (2000).
[103] A. Zibold, H.L. Liu, S.W. Moore, J.M. Graybeal, and D.B. Tanner, Phys. Rev. B **53**, 11 734 (1996).
[104] N. Ichikawa, S. Uchida, J.M. Tranquada, T. Niemöller, P.M. Gehring, S.-H. Lee, and J.R. Schneider, Phys. Rev. Lett. **85**, 1738 (2000).
[105] R.J. McQueeney, A.R. Bishop, Y.-S. Yi, and Z.G. Yu, J. Phys.: Condens. Matter **12**, L317 (2000); J. Tranquada, K. Nakajima, M. Braden, L. Pintschovius, and R. McQueeney, Phys. Rev. Lett. **88**, 075505 (2002).
[106] S. Chakravarty, H.-Y. Kee, and C. Nayak, Int. J. Mod. Phys. B **15**, 2901 (2001).
[107] P.A. Lee and X.G. Wen, Phys. Rev. Lett. **78**, 4111 (1997).
[108] J. Orenstein and A.J. Millis, Science **288**, 468 (2000).
[109] R.J. Gooding, Phys. Rev. Lett. **66**, 2266 (1991).
[110] D. Haskel, E.A. Stern, D.G. Hinks, A.W. Mitchell, J.D. Jorgensen, and J.I. Budnick, Phys. Rev. Lett. **76**, 439 (1996); D. Haskel, E.A. Stern, D.G. Hinks, A.W. Mitchell, and J.D. Jorgensen, Phys. Rev. B **56**, 521 (1997).
[111] V. Polinger, D. Haskel, and E. Stern, in *Vibronic Interactions* (Ref. 60), p. 215.
[112] J. Mesot, M.R. Norman, H. Ding, M. Randeria, J.C. Campuzano, A. Paramekanti, H.M. Fretwell, A. Kaminski, T. Takeuchi, T. Yokoya, T. Sato, T. Takahashi, T. Mochiku, and K. Kadowaki, Phys. Rev. Lett. **83**, 840 (1999).
[113] S. Ono, Y. Ando, T. Murayama, F.F. Balakirev, J.B. Betts, and G.S. Boebinger, Phys. Rev. Lett. **85**, 638 (2000); G.S. Boebin-

ger, Y. Ando, A. Passner, T. Kimura, M. Okuya, J. Shimoyama, K. Kishio, K. Tamasaku, N. Ichikawa, and S. Uchida, *ibid.* **77**, 5417 (1996).
[114] C. Quitmann, P. Almeras, J. Ma, R.J. Kelley, H. Berger, C. Xucyu, G. Margaritondo, and M. Onellion, Phys. Rev. B **53**, 6819 (1996).
[115] S. Ishihara, T. Egami, and M. Tachiki, Phys. Rev. B **55**, 3163 (1997).
[116] C.-Z. Wang, R. Yu, and H. Krakauer, Phys. Rev. B **59**, 9278 (1999).
[117] S. Tang and J.E. Hirsch, Phys. Rev. B **37**, 9546 (1988); **39**, 12 327 (1989); S. Mazumdar, *ibid.* **39**, 12 324 (1989); Q. Yuan, T. Nunner, and T. Kopp, Eur. Phys. J. B **22**, 37 (2001).
[118] M. Reedyk and T. Timusk, Phys. Rev. Lett. **69**, 2705 (1992).
[119] A.A. Aligia, M. Kulić, V. Zlatic, and K.H. Bennemann, Solid State Commun. **65**, 501 (1988); B. Normand, H. Kohno, and H. Fukuyama, Phys. Rev. B **53**, 856 (1996).
[120] H. Bilz, G. Benedek, and A. Bussmann-Holder, Phys. Rev. B **35**, 4840 (1987); A. Bussmann-Holder, A. Simon, and H. Büttner, *ibid.* **39**, 207 (1989).
[121] Q. Si, Y. Zha, K. Levin, and J.P. Lu, Phys. Rev. B **47**, 9055 (1993).
[122] A.A. Alligia, Phys. Rev. B **39**, 6700 (1987).
[123] O.K. Andersen, O. Jepsen, A.I. Liechtenstein, and I.I. Mazin, Phys. Rev. B **49**, 4145 (1994); A.I. Liechtenstein, O. Gunnarsson, O.K. Andersen, and R.M. Martin, *ibid.* **54**, 12 505 (1996).
[124] C. Falter, M. Klenner, and G.A. Hoffmann, Phys. Status Solidi B **209**, 235 (1998).